Journal of Materials Chemistry A

REVIEW

View Article Online
View Journal | View Issue

Check for updates

Cite this: J. Mater. Chem. A, 2024, 12, 12960

Multifunctional thermochromic smart windows for building energy saving

Dingkun Wang,† Guoqi Chen† and Jun Fu *

Windows are an important part of buildings and transmit light between indoors and outdoors. Frequent heat exchange through windows increases building energy consumption. Smart windows can change optical properties and modulate solar radiation, which are recognized as frontrunners in building energy saving. Among various smart windows, thermochromic windows usually passively regulate light transmittance in response to environmental temperature and have showed great potential for practical applications. Thermochromic materials are key to constructing thermochromic smart windows. Usually, a reversible phase transition takes place for thermoresponsive materials near the critical transition temperature, leading to changes in transmittance over different spectrum bands. Representative thermochromic materials include metal oxides, hydrogels, perovskites, ionic liquids, liquid crystals, *etc.* The intrinsic phase transition temperature, luminous transmittance, and solar modulation ability are among the critical parameters defining the performance of smart windows. New strategies have been developed to modulate the performance of thermochromic materials and smart windows to meet demands from different environments and climates. Such endeavors have boosted smart windows to modulate full-spectrum solar regulation and to achieve efficient all-climate building energy saving. Next generation smart windows will not only modulate solar transmission, but also convert and store solar energy through new power technologies such as thermoelectricity conversion and solar cells. Challenges and future prospects of smart windows are discussed to inspire future building energy saving.

Received 15th March 2024
Accepted 25th April 2024

DOI: 10.1039/d4ta01767f

rsc.li/materials-a

Published on 25 April 2024. Downloaded by Yunnan University on 8/6/2025 12:09:49 AM.

1. Introduction

Rapid development of the economy and technology boosts energy consumption in modern society. Building energy consumption accounts for 30–40% of the total in developed countries.[1,2] Common building energy services comprise heating, ventilation, and air conditioning.[3] Windows are considered the least energy efficient part of a building and account for

Key Laboratory of Polymeric Composite and Functional Materials of Ministry of Education, Guangdong Engineering Technology Research Centre for Functional Biomaterials, School of Materials Science and Engineering, Sun Yat-Sen University, Guangzhou, 510275, China. E-mail: fujun8@mail.sysu.edu.cn

† These two authors contributed equally.

Dingkun Wang

Dingkun Wang obtained his bachelor's degree in chemical engineering of forestry from Northwest A&F University in 2019 and a Master's degree in chemical engineering of forestry from the Chinese Academy of Forestry in 2023. He is currently pursuing a PhD degree supervised by Prof. Jun Fu at the School of Materials Science and Engineering, Sun Yat-sen University. His research interests include functional hydrogels for flexible electronics.

Guoqi Chen

Guoqi Chen obtained his bachelor's (2018) and Master's (2021) degrees from the College of Chemical Engineering, Fuzhou University. He is currently pursuing a PhD degree supervised by Prof. Jun Fu at the School of Materials Science and Engineering, Sun Yat-sen University. His research interests include functional hydrogels for smart windows and flexible electronic devices.

This journal is © The Royal Society of Chemistry 2024

Published on 25 April 2024. Downloaded by Yunnan University on 8/6/2025 12:09:49 AM.

about 50% of building energy consumption.[4] Therefore, smart windows are needed to regulate heat exchange to reduce energy consumption in buildings, which eventually facilitates a low-carbon economy.

Smart windows have been developed to intelligently regulate indoor solar radiation in response to external stimuli and consequently reduce heat exchange to conserve energy,[5,6] including electrochromic,[7] mechanochromic,[8] magnetochromic,[9] photochromic,[10,11] and thermochromic smart windows.[12,13] The former three types are known as active smart windows that need extra energy input to trigger and maintain the "ON" or "OFF" state. The latter two types are categorized as passive smart windows that spontaneously respond to environmental conditions without extra power input.

Thermochromic windows can modulate indoor solar irradiation by reversibly regulating the transmittance or reflectance of ultraviolet (UV, 250–380 nm), visible (380–780 nm) and near-infrared (NIR, 780–2500 nm) solar radiation.[14,15] Thermoresponsive materials that undergo phase transitions and reversible transparent-to-opaque transitions upon temperature changes have been utilized for thermochromic smart windows for solar modulation.[16,17] To date, many inorganic and organic thermochromic materials have been used for smart windows, including metal oxides[13,18,19] and hydrogels.[20–22] VO_2, for example, experiences a phase transition at 68 °C, above which the IR transmittance is decreased, while the transmittance in the visible band barely changes.[12,13,15] Besides, the solubility and/or hydrophilicity/hydrophobicity of polymer chains in thermochromic hydrogels can change at different temperatures, which causes a phase transition, chain conformation change, or precipitation of polymer chains.[20,23] Such transitions can cause variations in color or transparency to modulate solar modulation.[24,25] Other thermochromic materials, including ionic liquids, perovskites and liquid crystals, have also been used for thermochromic smart windows.[26]

Jun Fu

Dr. Jun Fu is a Professor at the School of Materials Science and Engineering at Sun Yat-sen University (SYSU). He obtained his BSc in applied chemistry at Wuhan University and PhD in polymer chemistry and physics from the Changchun Institute of Applied Chemistry, Chinese Academy of Sciences (CAS). He was a visiting scholar at the Max Planck Institute for Polymer Research and a research fellow at Massachusetts General Hospital/Harvard Medical School. He was appointed as a professor at the Ningbo Institute of Materials Technology and Engineering, CAS, and then moved to SYSU. His research focuses on high performance and functional hydrogels for smart windows, flexible wearables, and implantable devices.

The performances of smart windows are defined by several parameters including phase transition temperature (τ_c), luminous transmittance (T_{lum}), and solar modulation ability (ΔT_{sol}). τ_c determines the optimal working conditions and potential additional methods needed to trigger its transition. A transition temperature close to the target application conditions is desired. T_{lum} is important for daily use. High T_{lum} is desired when smart windows are not triggered to block solar radiation. ΔT_{sol} is defined as the solar transmittance change before and after the phase transition, which characterizes the ability to block solar energy. For light-harvesting smart windows, the power conversion efficiency (η) is a vital indicator that reflects the electrical output capability by converting the incident energy from the sun. The values of these parameters can be calculated using the following equations:

$$T_{lum} = \int \varphi_{lum}(\lambda) T(\lambda) d\lambda \Big/ \int \varphi_{lum}(\lambda) d\lambda \quad (1)$$

$$T_{sol} = \int_{250}^{2500} T(\lambda)\varphi(\lambda) d\lambda \Big/ \int_{250}^{2500} \varphi(\lambda) d\lambda \quad (2)$$

$$\Delta T_{sol} = T_{sol}(T < \tau_c) - T_{sol}(T > \tau_c) \quad (3)$$

$$\eta = \frac{J_{SC} \times V_{OC} \times FF}{P_{in}} \quad (4)$$

where $\varphi_{lum}(\lambda)$ represents the standard luminous efficiency function for visible light (380–780 nm), $T(\lambda)$ is the transmittance at wavelength λ, T_{sol} is the solar energy transmittance, J_{SC} is the short-circuit current density, V_{OC} is the open-circuit voltage, FF is the fill factor, and P_{in} is the incident light density.

Next generation smart windows are expected to harness solar energy instead of simply blocking and wasting it through scattering.[27,28] New concepts to integrate thermoelectricity conversion and solar cells in smart windows can harness solar energy and convert it into electricity, thus maximizing building energy exploitation.[28] Therefore, the next generation design principle of thermochromic smart windows requires intelligent management of incident sunlight according to temperature and rational utilization of solar light for power generation through photovoltaic technologies.

There are several review articles on thermochromic smart windows. Long's group has reviewed progress on thermochromic smart windows based on VO_2,[13] hydrogels,[20] and some other thermochromic materials.[12] Jin's group discussed thermochromic VO_2-based smart windows for practical applications.[29] Those review articles mainly focussed on single thermochromic materials for smart windows. Systematic and comparative investigations on smart windows based on different materials are needed to further discuss the influence of chemical structures, nanostructures, thermochromic properties, and device design on the thermochromic performance of smart windows, which will inspire novel strategies to develop high performance and functional smart windows to match application demands. In this review, we present a comprehensive review of high performance smart windows based on thermochromic materials. The intrinsic properties and response mechanisms of

Published on 25 April 2024. Downloaded by Yunnan University on 8/6/2025 12:09:49 AM.

representative thermochromic materials, including VO_2, hydrogels, ionic liquids, perovskites, and liquid crystals, and their applications to smart windows are discussed in detail (Fig. 1). Novel strategies ranging from molecule engineering to hybridizing, copolymerization, compositing, and nano-/microstructure engineering to develop high performance thermochromic materials to match application demands under diverse conditions and climates are introduced. In each section, current challenges and potential development directions are analyzed. Next generation smart windows by utilizing thermoelectricity conversion and solar cell technology to harness reflected solar energy for power generation are discussed (Fig. 1). Future development of thermochromic smart windows in building energy saving is discussed. This review aims to inspire research interest and innovations to promote the development of smart windows for building energy saving.

2. Thermochromic smart windows for solar modulation

Most thermochromic smart windows are based on thermoresponsive materials that undergo a phase transition at specific temperatures.[15] Such a phase transition induces either changes in crystal structures or phase separation that result in a transition from transparent to opaque status.[12] A variety of thermochromic materials have been used to fabricate smart windows.[8,14,20] The performances of smart windows highly rely on the transition temperature and transmittance in the UV-vis-infrared spectrum.[13,30] Great efforts have been made to modulate the transition temperature and transmittance to achieve autonomous transition and maximize solar modulation under mild conditions.[23,31]

2.1 Vanadium dioxide

2.1.1 Thermochromic mechanism. Vanadium is a transition element with a valence electron layer structure of $3d^3 4s^2$. It can form a variety of oxides, including VO, V_2O_3, VO_2, and V_2O_5. Only VO_2 undergoes a metal-to-insulator transition (MIT) at a critical temperature of 68 °C.[13,32] VO_2 is a polycrystalline metal oxide with a metastable phase, monoclinic phase (M), rutile phase (R), triclinic phase (T), *etc.*[33] At temperatures above 68 °C, VO_2 adopts the metallic rutile phase.[34,35] Therein, V^{4+} occupies the eight apexes and center of the unit cell (Fig. 2a). Besides, the V–V distance is equal to about 2.85 Å along the *c* axis. Below critical temperature, the VO_2 structure changes from R to M. V^{4+} migrates from the octahedron center to the outer surface. The V–V distances become 3.12 Å and 2.65 Å. The M phase VO_2 is insulating along the *c* axis.[13,36]

Currently, diverse mechanisms have been proposed for the phase transition of VO_2.[37–40] The electron–phonon interaction mechanism deems that the appearance of metallic rutile phase bandgap (R) comes from the distortion of the monoclinic phase (M).[41] The electron correlation mechanism suggests that the strong electron–electron correlation produces an insulating band gap.[42–44] The reversible phase transition of VO_2 (M/R) is described by using crystal field and molecular orbital theory (Fig. 2b). Briefly, in the rutile VO_2 (R), the 2p orbital of O^{2-} and 3d orbital of V^{4+} are hybridized to generate a narrow antibonding orbital π^* and a wide bonding π. Besides, V^{4+} offers

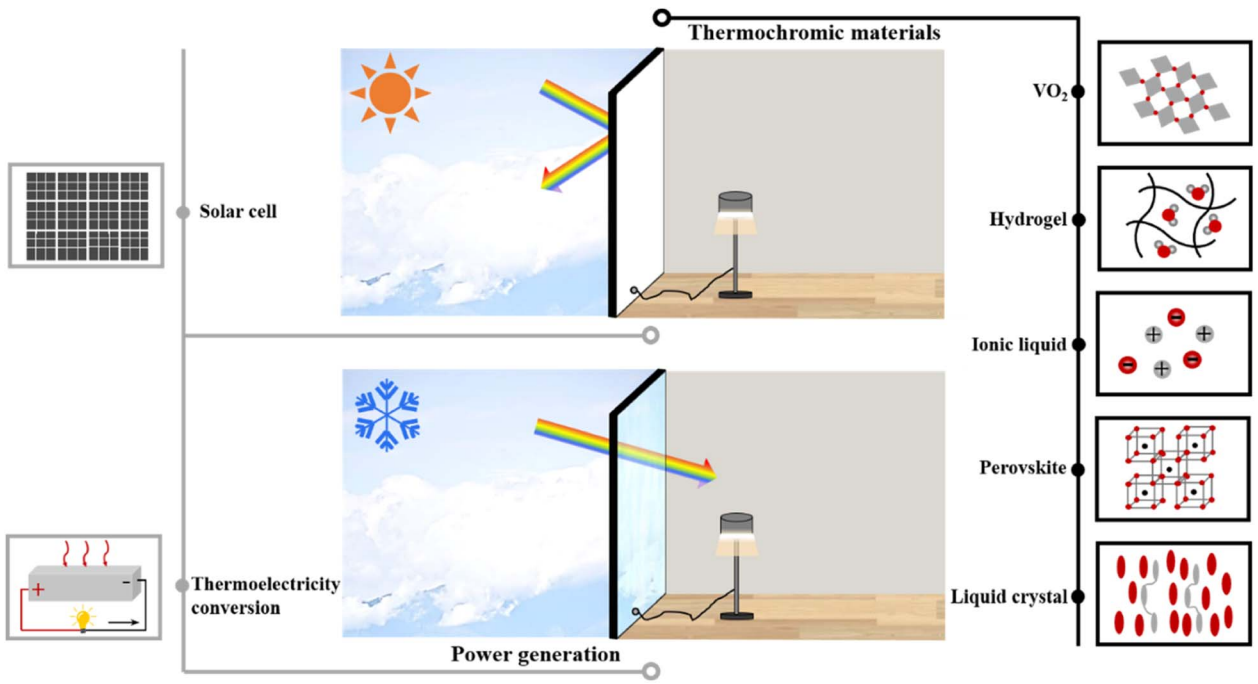

Fig. 1 Schematic outline of three components of smart windows in building energy saving: thermochromic materials, thermal exchange, and power generation. Thermochromic materials include VO_2, hydrogels, ionic liquids, perovskites, and liquid crystals. Power generation techniques involve thermoelectricity conversion and solar cell integration.

 This journal is © The Royal Society of Chemistry 2024

Published on 25 April 2024. Downloaded by Yunnan University on 8/6/2025 12:09:49 AM.

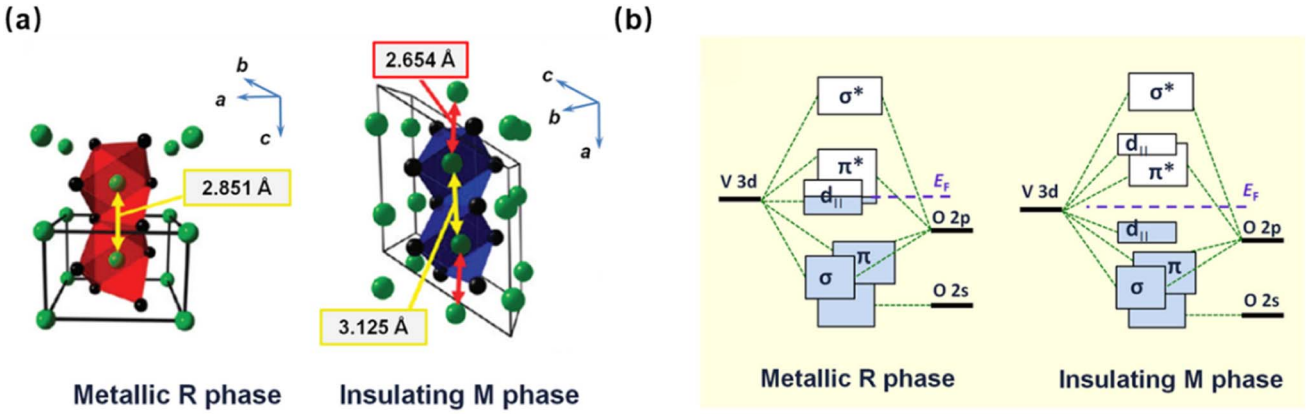

Fig. 2 (a) Schematic of the atomic structure for the metallic VO_2 R phase and the insulating VO_2 M phase. The V–V distances in each crystal structure are highlighted. Reproduced with permission from Whittaker *et al.*, J. Phys. Chem. Lett. 2, 745 (2011). Copyright 2011 American Chemical Society.[34] (b) Band structures of the metallic R and insulating M phases of VO_2 depicted by molecular orbital diagrams. Reproduced with permission from Cui *et al.*, Joule 2, 1707 (2018). Copyright 2018 Elsevier, Inc.[13]

an anti-bonding orbital $d_{//}$ parallel to the *c* axis. The semi-filled $d_{//}$ and π^* bands partially overlap at the Fermi level, showing metallic characteristics. But in the monoclinic VO_2 (M), the $d_{//}$ and π^* orbitals separate. The $d_{//}$ band splits into a filled orbital and an empty orbital with a band gap of 0.7 eV. Therefore, the electrons are trapped in the low energy $d_{//}$ orbital and VO_2 (M) becomes insulating.

2.1.2 High performance VO_2-based smart windows. VO_2 has always been the research hotspot in the field of smart windows due to its reversible phase transition temperature with prominent optical changes to modulate solar incident light. However, the high phase transition temperature,[13] limited luminous transmittance,[45] and weak solar modulation ability[46] have restricted the development of VO_2-based smart windows. Many strategies have been proposed to tackle these problems, including element doping,[46,47] multilayer films,[48,49] nanocomposite films,[50,51] and nano-/microstructural engineering.[52,53] For example, W can donate extra electrons to VO_2 and lower the thermal driving force for electronic movement. Thus, a W-doped VO_2 film has a lower τ_c of around 39 °C.[54] Multilayer VO_2 film containing functional layers, such as antireflection coating TiO_2,[55] can enhance T_{lum} to 45.0% and improve ΔT_{sol} to 12.1%. The VO_2/Si–Al gel nanocomposite film shows enhanced optical properties (T_{lum} of 59.0% and ΔT_{sol} of 12.0%) due to the relatively low refractive index of the Si–Al gel matrix and good dispersion of VO_2 particles.[56] A karst landform-like VO_2 film exhibits a higher T_{lum} of 61.3% and ΔT_{sol} of 11.9% than a continuous VO_2 film because of the localized surface plasmon resonance (LSPR) effect induced by the formation of isolated VO_2 nanoparticles.[57]

Thermochromic properties of representative VO_2-based materials for smart windows are summarized in Table 1. Elemental doping can lower the τ_c of VO_2 to about 20–50 °C, depending on the elements used. Meanwhile, the ΔT_{sol} of the VO_2 film can be improved to around 10–20% by constructing multilayer films. The T_{lum} of the VO_2 film can be increased to about 40–85% through fabricating nanocomposite films or nano-/microstructures. These results represent significant progress toward practical applications of VO_2-based smart windows.

2.1.2.1 Elemental doping. Elemental doping is used to reduce the critical phase transition temperature of VO_2.[13,15] Doping elements into VO_2 increases its electronic concentration and decreases the orbital splitting gap, which lowers the thermal driving force for electronic movement.[82] On the other hand, the doping elements partly occupy the positions of V or O and thus destroy the V–V chain in the monoclinic structure.[83] As a result, τ_c decreases. Many elements, including H,[60] W,[58] Zr,[61] Mg,[63] Hf,[64] Ta,[47] *etc.*, are used to dope VO_2. For example, H doping leads to the formation of a typical H–O covalent bond, which distorts the V–V bonds (Fig. 3a).[60] Thus, the H-doped VO_2 is prone to a phase transition at relatively lower temperatures (τ_c) as reduced by 38 K/at% H. Similarly, τ_c can be lowered by doping the W element. A sputtered $V_{0.982}W_{0.018}O_2$ layer deposited on an ultrathin flexible glass substrate shows an ultralow τ_c of 22 °C.[58] A W-doped VO_2 layer sandwiched by two SnO_2 layers deposited on glass substrates through pulsed laser deposition exhibits a τ_c of 39 °C. Interestingly, the ΔT_{sol} and T_{lum} of this film are increased from 2.6% to 10.7% and from 45.0% to 54.4%, respectively.[54] Zr has lower electronegativity (1.33) than V (1.63) and therefore can serve as a donor in VO_2. A W/Zr co-doped VO_2 film prepared by the hydrothermal reaction and spin-coating shows a τ_c of 46.9 °C. W doping weakens the transition temperature, and Zr widens the energy band gap. This method simultaneously shifts the absorption edge and enhances ΔT_{sol} and T_{lum}.[61] Similarly, combined doping with W and Mg decreases τ_c to 36.9 °C and enhances ΔT_{sol} to 10.8% and T_{lum} to 46.2%.[63] Similar Hf–W co-doping reduces the τ_c of the VO_2 film to 38.9 °C, together with a ΔT_{sol} of 13.1% and T_{lum} of 41.1%.[64] Hf–W co-doping shortens the V–V bond because of the higher ion valence of W^{6+} than V^{4+} (Fig. 3b). W can donate extra electrons to VO_2 and thus reduce τ_c. Specifically, HfO_2 has a wider optical bandgap (5.7 eV) than pure VO_2 (2.5 eV). Therefore, the Hf^{4+}-doped VO_2 film has a widened

Published on 25 April 2024. Downloaded by Yunnan University on 8/6/2025 12:09:49 AM.

Table 1 Thermochromic properties of VO_2 based on different modification strategies

Category	Materials/structures	T_{lum} (%)	ΔT_{sol} (%)	τ_c (°C)	Ref.
Element doping	W-doped VO_2 coating	45.0	10.0	22.0	58
	W-doped VO_2 film	54.4	10.7	39.0	54
	Zr-doped VO_2 film	61.4	10.3	—	59
	Mg-doped VO_2 film	59.4	9.5	—	59
	Si-doped VO_2 film	54.7	13.9	—	46
	H-doped VO_2	—	—	30.0	60
	W/Zr co-doped VO_2 film	60.7	10.6	46.9	61
	SiO_2/W co-doped VO_2 film	60.0	—	—	62
	W/Mg co-doped VO_2 film	46.2	10.8	36.9	63
	Hf/W co-doped VO_2 film	41.1	13.1	38.9	64
	SiO_2/VO_2 double-layered film	55.0	—	70.0	65
	VO_2/TiO_2 double-layered film	61.5	15.1	—	66
	VO_2/TiO_2 double-layered structure	49.0	7.0	—	67
	Si–Al/VO_2 double-layered coating	44.0	18.9	—	68
Multilayer films	TiO_2/VO_2/TiO_2/VO_2/TiO_2 multilayered film	45.0	12.1	60.0	55
	SiN_x/NiCr/$NiCrO_x$/VO_x/$NiCrO_x$/NiCr/SiN_x multilayered film	40.5	18.4	54.0	48
	SiN_x/VO_2/SiN_x multilayered film	40.4	14.5	—	49
	SiO_2/VO_2/SiO_2/polymer multilayered coating	54.0	16.4	—	69
	WO_3/VO_2/WO_3 multilayered structure	55.4	—	52.0	70
Nanocomposite films	VO_2 nanoparticles in a Ni-based thermochromic system	73.4	18.2	—	71
	VO_2 nanoparticles and Sb-doped SnO_2 nanoparticles	60.1	20.0	66.3	72
	VO_2 nanoparticles and Sb-doped SnO_2 nanoparticles	84.4	11.6	84.5	72
	HfO_2/VO_x nanocomposite film	51.6	15.4	60.6	73
	VO_2 nanoparticles with SiO_2 aerogel particles	41.2	18.4	—	74
	VO_2 nanoparticles in a polyurethane matrix (single layer)	54.0	14.5	—	50
	VO_2 nanoparticles in a polyurethane matrix (three layers)	46.8	20.0	—	50
	VO_2 nanoparticles in polyvinyl butyral	43.4	17.3	—	51
	Core–shell VO_2@SnO_2 nanoparticles	47.5	25.0	~65.0	75
	VO_2 nanoparticles in a polyvinyl pyrrolidone matrix	57.3	13.8	—	76
	W-doped VO_2 nanoparticle film	50.0	10.0	32	77
	Double-layered nanoparticle array of VO_2	46.1	13.2	—	78
Nanostructure/microstructure	Three-dimensional ordered microporous VO_2	71.1	10.8	—	52
	Nanoporous VO_2 film	78.0	14.1	—	79
	VO_2 nanoparticles film with VO_2 clusters	46.3	11.2	—	80
	VO_2 mesh film	86.0	—	—	81
	Micro-patterned VO_2 film	43.3	14.9	—	53

thermoresponsive optical bandgap, which is attributed to a high T_{lum}. Element doping is feasible to lower the transition temperature, regulate the transmittance, and improve solar modulation of VO_2.

2.1.2.2 Multilayer films. Moreover, designing multilayer films is an important way to improve the optical properties of a VO_2 film.[13,15,84] To start with, a single functional layer is commonly introduced to improve the luminous transmittance of a pure VO_2 film. For example, a thin SiO_2 layer (about 100–300 nm) on top of a VO_2 film increases T_{lum} from 42% to 55% at 650 nm.[65] TiO_2 with a high refractive index[85] of 2.2 serves as an antireflection coating to increase the T_{lum} (from 40.3% to 61.5%).[66] The film thickness is important. An optimal VO_2 (50 nm)/TiO_2 (40 nm) structure is reported with a high luminous transmittance of 49%.[67] Anti-reflection can be achieved by micro-patterning the VO_2 film to simultaneously modulate ΔT_{sol} and T_{lum}. The refractive index bilayer film is responsive to temperature variation,[68] which presents a higher solar transmittance at lower temperature with enhanced T_{lum} (from 39% to 44%) (Fig. 4a).

Multilayer structures balance the trade-off between ΔT_{sol} and T_{lum} and further promote the solar modulation ability. A SiN_x/NiCr/$NiCrO_x$/VO_x/$NiCrO_x$/NiCr/SiN_x multilayer film deposited on a glass substrate shows a solar modulation of 18.4% and luminous transmittance of 40.5%.[48] The multilayer SiN_x/VO_2/SiN_x film consisting of a ~80 nm VO_2 layer and two SiN_x layers has enhanced solar modulation from 10.8% to 14.5% and luminous transmittance from 36.1% to 40.4% (Fig. 4b).[49] Moreover, a dip-coated four-layered SiO_2/VO_2/SiO_2/polymer film exhibits a solar modulation of 16.4% and luminous transmittance of 54.0%.[69] Furthermore, a three-layer Ag/VO_2/Pt film is fabricated as a metal–dielectric–metal structure (Fig. 4c).[86] The trilayer film shows a VO_2 thickness-dependent reflective color. As the insulating VO_2 layer undergoes a phase transition, the reflective color changes in response to temperature changes, leading to a unique solar modulation ability (Fig. 4c).

2.1.2.3 Nanocomposite films. Furthermore, compositing VO_2 nanoparticles with other functional materials can improve the optical properties.[71,79,87] For example, a nanocomposite film of VO_2 and a Ni-based ligand exchange thermochromic system (NLETS) presents a 127% increase from 8.02% to 18.19% in

 This journal is © The Royal Society of Chemistry 2024

Published on 25 April 2024. Downloaded by Yunnan University on 8/6/2025 12:09:49 AM.

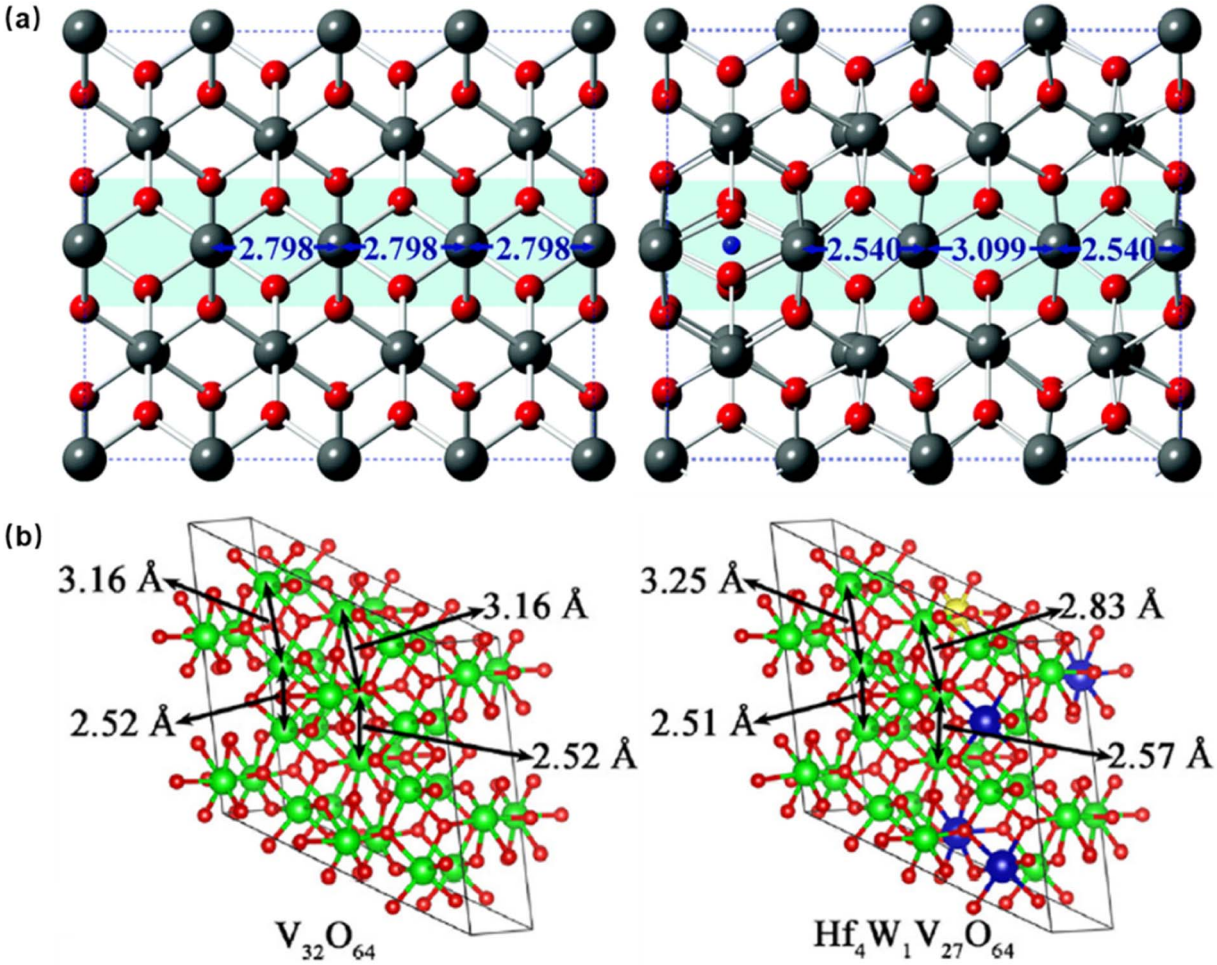

Fig. 3 (a) The V–V chains along the *c* axis in pure and H-doped VO_2 (R). Reproduced with permission from Cui *et al.*, Phys. Chem. Chem. Phys. 17, 20998 (2015). Copyright 2015 Royal Society of Chemistry.[60] (b) The calculated super-cell structures of pure $V_{32}O_{64}$ and $Hf_4W_1V_{27}O_{64}$. Reproduced with permission from Wang *et al.*, Appl. Phys. Lett. 118, 192102, (2021). Copyright 2021 American Institute of Physics.[64]

ΔT_{sol} at a high T_{lum} (73.36% at 20 °C and 68.71% at 90 °C).[71] The VO_2 nanoparticles are uniformly distributed in the film. The NLETS has a macroscopic color change (from transparent to light blue) as temperature is increased, which thereby enhances the solar modulation ability of the nanocomposite film. A nanocomposite film containing VO_2 nanoparticles and Sb-doped SnO_2 (ATO) nanoparticles increases T_{lum} from 39% to 84% at a ΔT_{sol} of 11.57%.[72] ATO nanoparticles are distributed on the surfaces and interstices of VO_2 nanoparticles, which widens the optical band gap of VO_2 nanoparticles and thus improves the luminous transmittance of the film.

SiO_2 is often used to modify the optical performances of pure VO_2 films because of its outstanding visible transparency and low-cost coating process.[13] VO_2/SiO_2 composite films are constructed through a facial mechanical ball-milling technology (Fig. 5).[74] The SiO_2 aerogel particles are coated on VO_2 particles to prevent aggregation, which enhances the solar modulation (ΔT_{sol} = 18.4%) and luminous transmittance (T_{lum} = 41.2%). Similarly, VO_2 is composited in polyurethane with good dispersion and exhibits enhanced solar modulation from 6.6% to 14.5% and a luminous transmittance of 54%.[50] However, the abovementioned research focuses on enhancing luminous transmittance and solar modulation ability of VO_2. The high phase transition temperature of VO_2 is rarely addressed. New VO_2-based thermoresponsive materials with both moderate transition temperatures and excellent dispersion could be anticipated by compositing element-doped VO_2 nanoparticles into matrices.

2.1.2.4 Nano-/microstructure engineering. Nano-/microstructure engineering is another effective strategy to modulate the thermochromic performances of VO_2.[15] Ordered or periodical nano-/microscale distribution of VO_2 has superior thermochromic properties compared with that of randomly distributed VO_2.[29,88] For example, two-dimensional ordered VO_2 nanostructures are fabricated by infiltrating VO_2 precursor solution into colloidal crystal templates.[78] By adjusting the fluidity of the VO_2 precursor and separation distance of template spheres, VO_2 nanoparticles, nanodomes and nanonets are fabricated on substrates.[89] The two-dimensional ordered VO_2 nanoparticle array presents a luminous transmittance of 46.1% and solar modulation ability of 13.2%. The nanoparticle array has a porosity-induced luminous transmittance

Published on 25 April 2024. Downloaded by Yunnan University on 8/6/2025 12:09:49 AM.

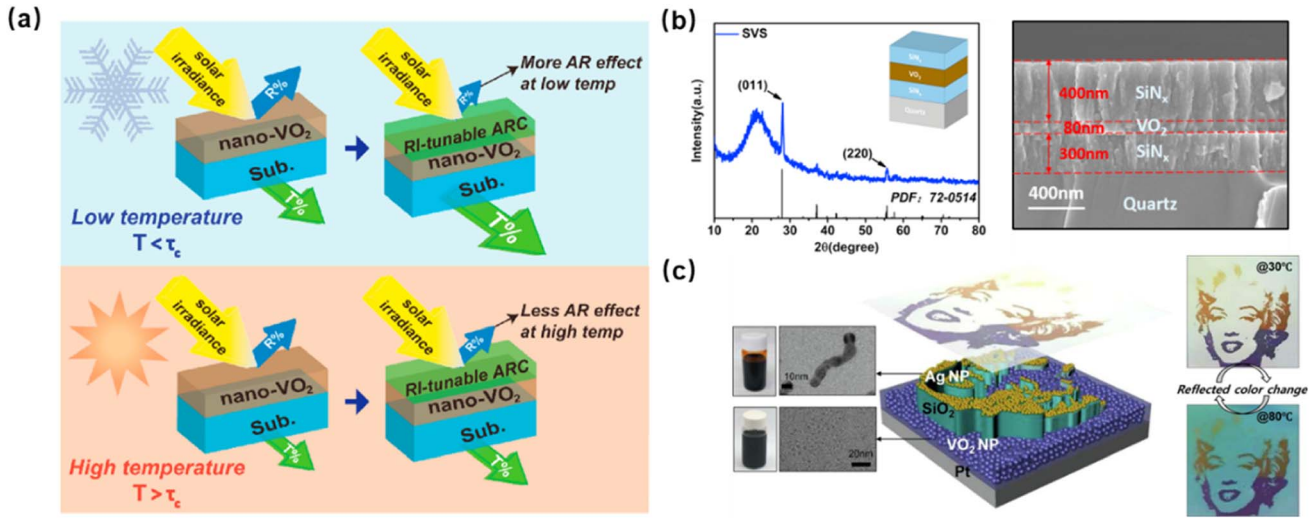

Fig. 4 (a) Schematic illustration of the refractive index-tunable bilayer film with nano-VO_2. Reproduced with permission from Liu *et al.*, J. Alloys Compd. 731, 1197 (2018). Copyright 2018 Elsevier, Inc.[68] (b) XRD pattern and cross-section SEM image of a multilayer $SiN_x/VO_2/SiN_x$ film. Reproduced with permission from Long *et al.*, Sol. Energy Mater Sol. Cells 189, 138 (2019). Copyright 2019 Elsevier, Inc.[49] (c) Three-layered Ag/VO_2/Pt film and Marilyn Monroe's image composed of different SiO_2 thicknesses at different temperatures. Reproduced with permission from Kim *et al.*, Appl. Surf. Sci. 565, 150610 (2021). Copyright 2021 Elsevier, Inc.[86]

strengthening and a temperature-response LSPR effect, which is helpful to enhance the solar modulation ability because the LSPR intensity is increased at high temperatures, leading to higher absorption and lower transmittance.

Apart from ordered VO_2 structures, random VO_2 nanoporous structures with the LSPR effect can also improve luminous transmittance and solar modulation ability. VO_2 films with spontaneous random nanoporous structures are prepared to enhance the optical performances (ΔT_{sol} = 14.1% and T_{lum} = 78%) (Fig. 6a).[79] The VO_2 film with random teeth-like nanoparticles and nanopores enhances absorption of LSPR in the NIR range and thus increases the T_{lum} and ΔT_{sol}. The T_{lum} of VO_2 films at different incident angles is enhanced by structure design. Similarly, a VO_2 film with random large pores and isolated optical interaction particles is obtained by intense pulsed light (IPL) sintering to regulate light transmittance performance (Fig. 6b).[80] The film sintered at 2000 V presents a visible light transmittance of 63.6% at 550 nm and luminous transmittance over 46.3%.

2.2 Hydrogels

2.2.1 Thermochromic mechanism. Hydrogels comprise a three-dimensional crosslinked polymer network with infiltrated water, behaving like both liquids and solids,[90–92] and usually possess mechanical flexibility, softness, permeability, and conductivity. Thermochromic hydrogels undergo phase separation and transparent-to-translucent transitions upon temperature changes, which have been utilized for smart windows.[93–98]

Hydrogels may have the upper critical solution temperature (UCST) and the lower critical solution temperature (LCST). Above LCST or below UCST, polymer chains in the hydrogel network are less soluble and adopt collapsed conformation or phase separated microdomains that scatter incident light. As a result, hydrogels appear opaque or translucent. At temperatures below LCST or above UCST, the polymer chains become soluble and swollen and the hydrogels become transparent.

LCST hydrogels at temperatures below τ_c are transparent and allow incident light to easily pass through thermochromic hydrogels (Fig. 7).[23] However, at temperatures above τ_c, the hydrophobic polymer chains contract and aggregate to resist hydrophilic water molecules, and then phase separation occurs inside the hydrogels to form collapsed polymer clusters that can effectively scatter incident light to impair the visible transmittance of hydrogels. This is fundamental for solar modulation of thermochromic hydrogels.

2.2.2 LCST hydrogels. Poly(*N*-isopropylacrylamide) (PNIPAM) hydrogels are a typical LCST hydrogel that undergoes a phase transition from hydrophilic to hydrophobic at 32 °C.[16] Above 32 °C, PNIPAM chains become hydrophobic and less soluble and adopt a collapsed conformation and form globules that scatter solar light.[98,99] This is the basis for PNIPAM hydrogels to serve as smart window materials to modulate solar incidence.

Zhou *et al.* reported the first PNIPAM hydrogel-based smart windows with a τ_c of around 32 °C.[100] The luminous transmittance of hydrogel films decreases with an increase in thickness and shows an optimal T_{lum} of 70.7% at 52 μm thickness. The PNIPAM hydrogel-based smart window becomes opaque above τ_c and shows a ΔT_{sol} of 25.5%. It is needed to modulate the intrinsic phase separation behavior of PNIPAM to further improve both the T_{lum} and ΔT_{sol} for high performance thermochromic smart windows.

One solution is to modulate the scattering behavior of PNIPAM-based hydrogels. Fang *et al.* synthesized microparticles of a poly(*N*-isopropylacrylamide)-2-aminoethylmethacrylate

 This journal is © The Royal Society of Chemistry 2024

Published on 25 April 2024. Downloaded by Yunnan University on 8/6/2025 12:09:49 AM.

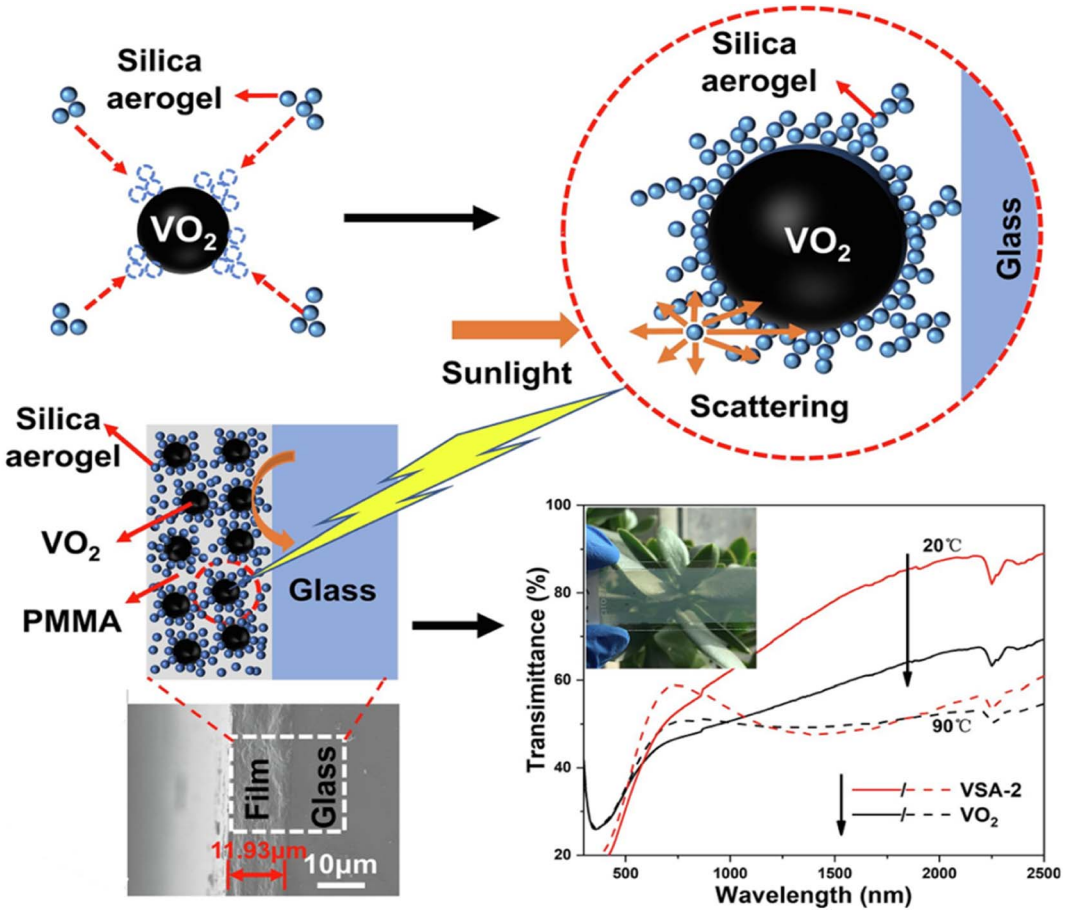

Fig. 5 The mechanism of solar transmission increment of a VO_2/SiO_2 composite film. Reproduced with permission from Kang *et al.*, Appl. Surf. Sci. 573, 151507 (2022). Copyright 2022 Elsevier, Inc.[74]

hydrochloride (PNIPAM-AEMA) copolymer with large diameters and uniform crosslinks.[16] The large particle size (~1388 nm) and homogeneous internal structures with a very low light scattering contrast provide a high T_{lum} of 87.2% at 25 °C (Fig. 8a). In contrast, the particles shrink to about 546 nm at 35 °C, which scatter light over a broad spectrum, and thus show a high ΔT_{sol} of 81.3% (Fig. 8b).

A homogeneous hydrophilic network, and thus high T_{lum}, can be further achieved by introducing hydrophilic chains through free radical polymerization at low temperatures to avoid unwanted phase separation induced by reaction heating.

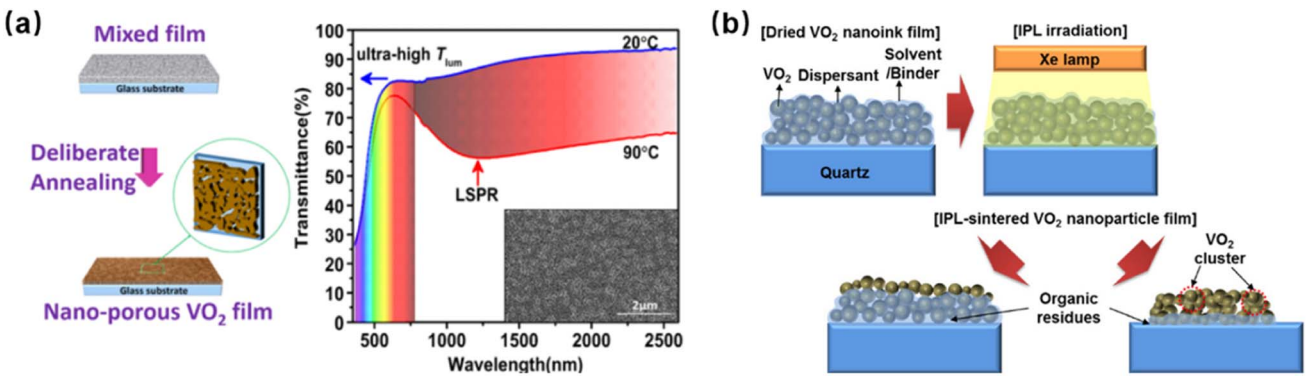

Fig. 6 (a) Schematic diagram of fabrication route for nanoporous VO_2 and optical properties of nanoporous VO_2 films. Reproduced with permission from Long *et al.*, ACS Appl. Mater. Interfaces 11, 22692 (2019), Copyright 2019 American Chemical Society.[79] (b) Schematic illustration of VO_2 nanoparticle films prepared by intense pulsed light and spin coating. Reproduced with permission from Kim *et al.*, Mater. Des. 176, 107838 (2019). Copyright 2019 Elsevier, Inc.[80]

Published on 25 April 2024. Downloaded by Yunnan University on 8/6/2025 12:09:49 AM.

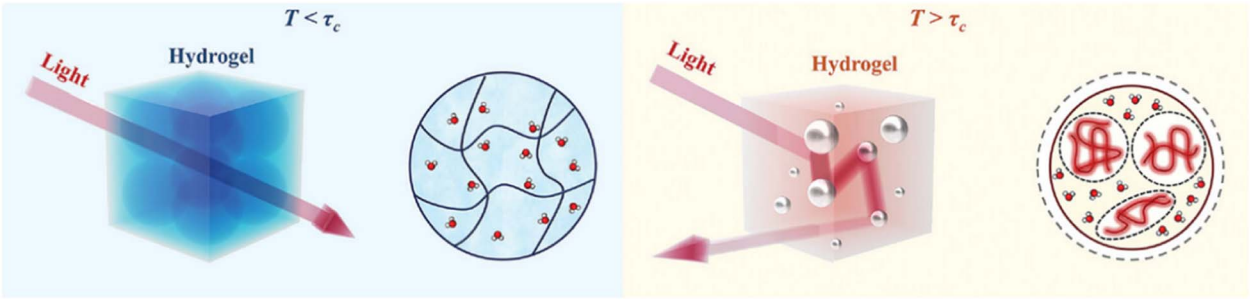

Fig. 7 Schematic illustration of thermochromic mechanism of thermochromic hydrogels. Reproduced with permission from Chen *et al.*, Adv. Mater. 35, 2211716 (2023). Copyright 2023 Wiley-VCH GmbH.[23]

Hydrophilic hydroxypropylmethyl cellulose (HPMC) is mixed with *N*-isopropylacrylamide for free radical polymerization at 0 °C.[97] The heat released during the polymerization process could be dispersed in time. No phase separation takes place as that observed during high temperature-induced free radical polymerization of *N*-isopropylacrylamide. Here, the abundant hydroxyl groups of HPMC could form extensive hydrogen bonds with PNIPAM chains and water. The PNIPAM and HPMC chains form a uniform distribution, leading to a high transparency T_{lum} of 90.8% at low temperature.

A hydroxypropyl cellulose (HPC) hydrogel is another important LCST hydrogel.[101–103] It possesses both hydrophobic epoxy ether groups and hydrophilic hydroxyl groups and has a miscible–immiscible transition at 42 °C.[104,105] The random coil chains of HPC transform into collapsed spheres above 42 °C, resulting in an opaque phase that scatters solar radiation. The high LCST of HPC presents solar modulation at temperature much higher than the comfortable room temperature.

Zhang *et al.* constructed smart windows by using a hydroxypropyl cellulose-polyacrylic acid (HPC-PAA) hydrogel (Fig. 9a). The LCST of the HPC-PAA hydrogel is sensitive to solution pH and can be tuned down to 26.5 °C at pH 2.5.[106] The hydrogel has massively interlaced pores (~13 μm) because of the incorporation of PAA. The enlarged pores with a low scattering contrast increase T_{lum} to 90.1% at 18 °C. The pore diameter is reduced due to phase separation at 40 °C, which enhances light scattering, and thus the hydrogel shows a ΔT_{sol} of 47.5%. Afterwards, photothermal cesium tungsten oxide ($Cs_{0.32}WO_3$) nanoparticles are further introduced to the HPC-PAA hydrogel to enhance NIR shielding performance (Fig. 9b).[107] $Cs_{0.32}WO_3$ can transform the absorbed NIR light into heat through local surface plasmon resonance. Thus, the composite hydrogel reduces the NIR transmittance from 81.7% to 41.6% at 22 °C.

Combining the temperature-responsive hydrogel mechanism with other mechanisms can endow smart windows with richer modulation abilities. Gao *et al.* constructed a smart

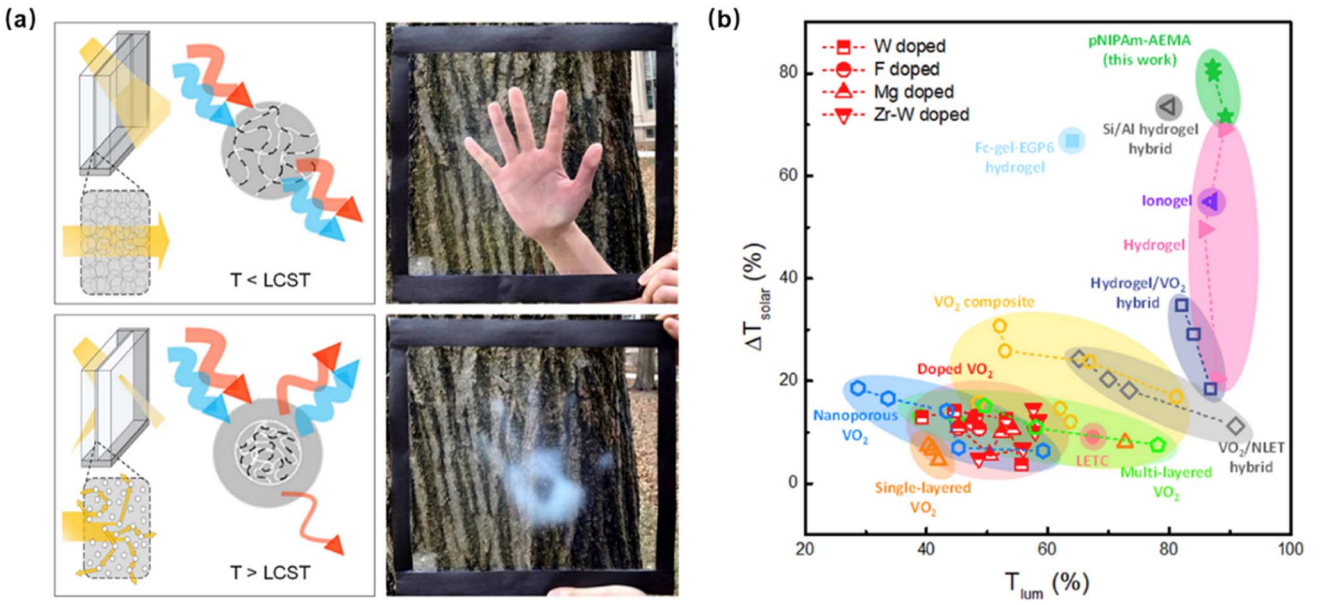

Fig. 8 (a) The phase transition of the PNIPAM-AEMA hydrogel-based smart window triggered by the hand. (b) Thermochromic performances of PNIPAM-AEMA hydrogel and other reported materials. Reproduced with permission from Li *et al.*, Joule 3, 290 (2019). Copyright 2019 Elsevier, Inc.[16]

 This journal is © The Royal Society of Chemistry 2024

Published on 25 April 2024. Downloaded by Yunnan University on 8/6/2025 12:09:49 AM.

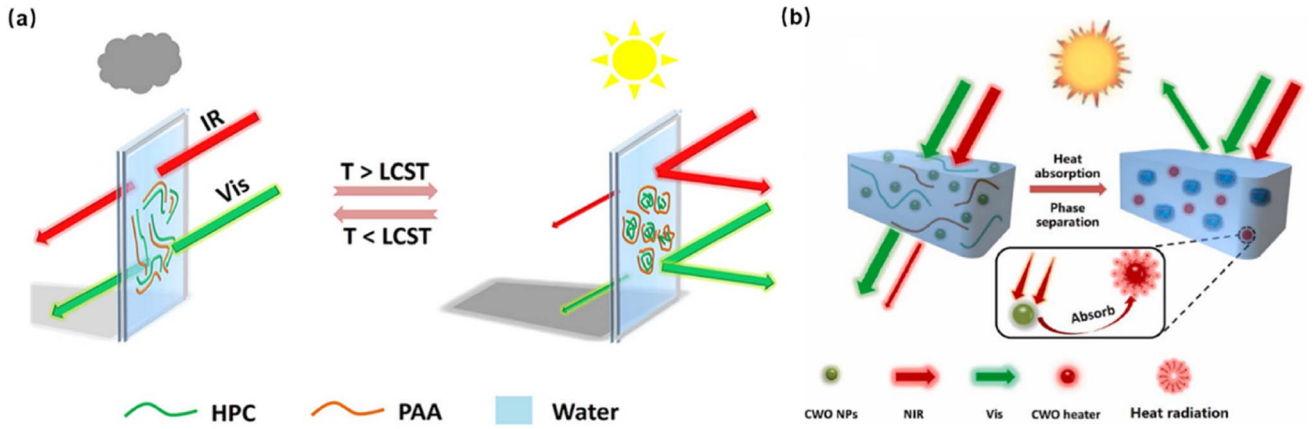

Fig. 9 (a) The transmittance modulation mechanism of HPC-PAA hydrogel. Reproduced with permission from Zhang *et al.*, ACS Appl. Energy Mater. 4, 9783 (2021), Copyright 2021 American Chemical Society.[106] (b) The schematic illustration of the phase separation of photothermal nanoparticles-embedded HPC-PAA hydrogel. Reproduced with permission from Zhang *et al.*, Ceram. Int. 48, 37122 (2022). Copyright 2022 Elsevier, Inc.[107]

window of HPC-PAA hydrogel doped with H^+ and Li^+.[108] The phase transition temperature is adjusted through changing the hydrogen bond between molecular chains by ion doping. By integrating the ion doped thermochromic HPC-PAA hydrogel layer with the electrochromic WO_3-indium tin oxide (ITO) layer, the smart window possesses four reversibly switch modes: transparent state, thermochromic state, electrochromic state, and electrothermal dual response state. Thus, the HPC-PAA hydrogel-based smart window shows a electric-/thermal-dual response.

2.2.3 UCST hydrogels. Polyampholyte (PAH) hydrogels are a typical UCST material.[22,109] Above UCST, the ionic bonds are broken and the polymer chains become soluble. The polymer chains aggregate and separate from water below UCST. Thus, PAH exhibits a reversible optical transition from transparency to opaqueness.[110]

Chung *et al.* reported a highly flexible smart window based on PAH hydrogels that allows visible light to transmit at high temperature and blocks mid-infrared radiation at low temperature.[109] Such smart windows not only protect personal privacy but also prevent heat loss through blackbody radiation. A hydrophobic monomer (3-(methacryloylamino)propyl)trimethylammonium chloride (MPTC) is introduced to modulate the phase separation behavior of PAH. The PAH-MPTC hydrogel presents a phase transition temperature of 43.4 °C. The particle size (~1 μm) and homogeneous pore structures at 55 °C provide a transmittance of 82% at 800 nm wavelength. The hydrogel with bubble-like porous structures (~40 μm) at 20 °C represents

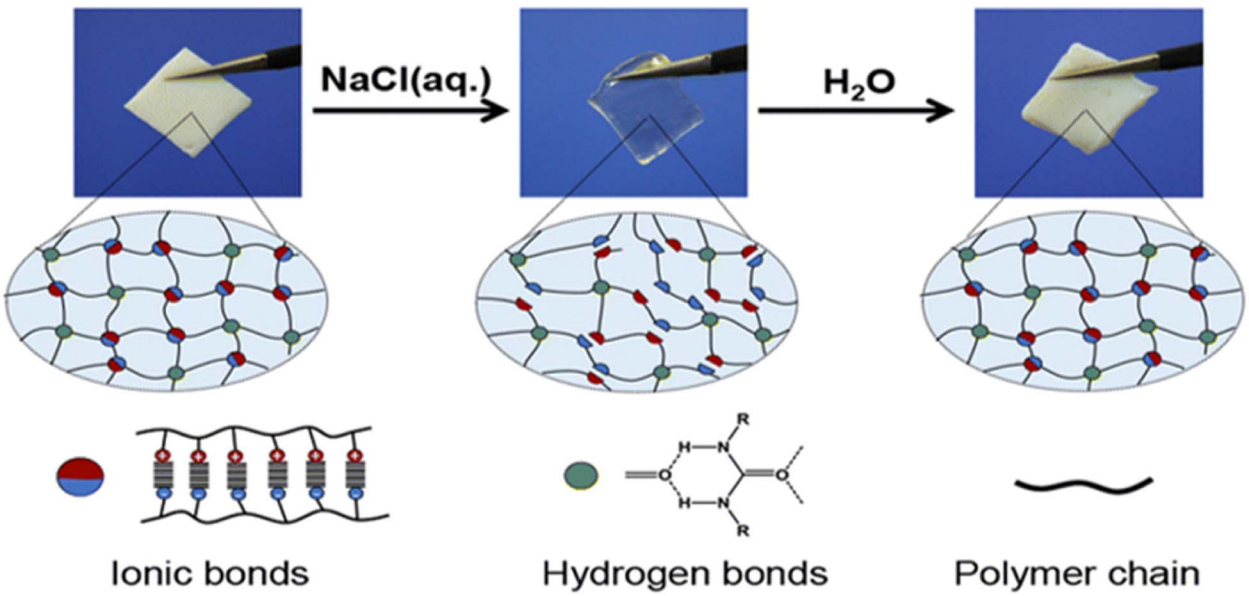

Fig. 10 Pictures of PAH hydrogel in opaque and transparent states when immersed in H_2O and NaCl(aq), respectively, and the proposed dynamic nature of ionic bonds. Reproduced with permission from Guo *et al.*, Mater. Horizons 9, 3039 (2022). Copyright 2022 Royal Society of Chemistry.[22]

Published on 25 April 2024. Downloaded by Yunnan University on 8/6/2025 12:09:49 AM.

macroscopic phase separation, leading to a good mid-infrared modulation ability. By combining a printed electrical heater with the PAH-MPTC hydrogel, this PAH hydrogel-based smart window could be actively controlled. It is necessary to induce the phase separation of PAH without electrical energy input to achieve active control of smart windows.

Salt can be used to trigger PAH hydrogel-based smart windows.[22] Since the phase separation of PAH is dominated by ionic bonds and dense entanglement to scatter natural light (Fig. 10), when PAH is immersed in sodium chloride solution [NaCl(aq)], the ionic bonds in PAH are disassociated. Thus, the polymer chain associates are partially ruptured, and the entanglement density decreases to pass through incident light, leading to a T_{lum} of 92%. Subsequently, the PAH hydrogel automatically recovers its opaqueness within 20 minutes when transferred from NaCl(aq) to H_2O. The reversible transparency-shifting endows the PAH hydrogel with a ΔT_{sol} of 88%.

2.2.4 High performance hydrogel-based smart windows. Thermochromic hydrogels are considered the most promising and competitive materials for smart windows and have attracted increasing research interest in the field of building energy saving.[15,20,111,112] However, current challenges of hydrogel-based smart windows include fixed transition temperature,[23] limited solar modulation ability,[12] poor mechanical strength,[15] and low-temperature freezing.[95] The τ_c of most thermochromic hydrogels is fixed and does not satisfy intricate weather conditions. The solar modulation of hydrogels in the NIR region is lower than that of VO_2. Pure hydrogels are mechanically fragile and usually freeze at temperatures below the freezing point of water. Methods have been proposed to tackle these problems[15,113] by introducing functional materials,[114,115] regulating structure configuration,[116,117] and developing liquid smart windows.[21] For example, the phase separation of HPC is susceptible to inorganic salts because of the weakened hydrogen bonds between polymer chains and water.[102] Thus, the τ_c of HPC could be reduced from 42 °C to 30 °C by introducing NaCl. A supramolecular alcogel containing host-cellulose and guest-PAAM shows an excellent tensile strength of 13.6 MPa.[116] The addition of glycerol breaks the hydrogen bond between water molecules and inhibits the crystallization of water, resulting in smart windows with freezing tolerance at −18 °C.[118]

Thermochromic properties and characteristics of these thermosensitive hydrogels are shown in Table 2. The performances of hydrogels and related smart windows can be flexibly modulated over a broad range, including adjustable τ_c (16.0–43.5 °C), strong solar modulation ability (33.4–89.9%), good mechanical strength (89.5 kPa–5.58 MPa tensile strength), and anti-freezing capability (−18 to −100 °C freezing point). Unlike metal oxides, hydrogels are soft materials with excellent processibility and adaptiveness to match specific application demands, even at temperature far below the freezing point.

Table 2 Thermochromic properties and characteristics of various thermosensitive hydrogels

Materials	Characteristic	T_{lum} (%)	ΔT_{sol} (%)	τ_c (°C)	Ref.
PNIPAM	Decent visible transmittance	70.7	25.5	32.0	100
PNIPAM/AEMA	Low-cost and scalable fabrication process	87.2	81.3	32.0	16
PNIPAM/HPMC	Good solar modulation capability	90.8	81.5	32.0	97
HPC	First smart window based on HPC hydrogel	67.4	25.7	30.0	102
HPC/PAA	Reduced LCST by modulating pH	90.1	47.5	26.5	106
HPC/PAA	Reduced LCST by modulating pH, and outstanding cycling stability	91.8	73.7	25.8	107
HPC/PAA	Reduced LCST by modulating pH	90.1	80.0	35.2	119
HPC/PAA	Electric-/thermal-dual-responsive	89.0	59.0	—	108
PAAM/SDS	Adjustable LCST in the range of 16–34 °C	85.0	—	16.0	120
PAAM/C_{18}/SDS	Adjustable LCST in the range of 20–50 °C	99.0	33.4	20.0	121
PNIPAM/NaCl	Adjustable LCST in the range of 31.7–24.5 °C	95.1	89.9	27.2	122
PNIPAM/DMMA	Adjustable LCST in the range of 32.5–43.5 °C	91.3	88.8	32.5	23
PNIPAM/Ethanol	Enhanced solar modulation ability and solar shielding	89.9	71.8	28.0	123
PNIPAM/HA	Enhanced visible transmittance and solar modulation ability	85.9	68.6	32.0	114
W-VO_2/PNIPAM/HPC	Enhanced solar modulation ability	87.2	65.7	29	124
PNIPAM particles/water	Revolutionarily liquid smart window for enhancing optical properties	90	68.1	32.5	21
PNIPAM/PAA chain/microparticle hybrids suspension	Liquid smart window for enhancing solar modulation ability	91.5	85.8	26.7	112
SPU/binary ionic liquid	Enhanced mechanical strength by hydrogen bonds	95.1	83.0	—	115
PNIPAM/ACMO	Enhanced mechanical strength by 3D printing technology	85.8	79.3	—	99
PNIPAM/PDMAA/EG	Excellent anti-freezing ability and adjustable LCST	89.3	80.7	~30.0	125
PNIPAM/glycerol	Good anti-freezing ability and adjustable LCST	90.0	60.8	~26.0	118
PNIPAM/HPC	Good anti-freezing ability	80.7	64.5	~29.0	95
PNIPAM microgel	High luminous transmittance and fast response time	91.2	81.8	—	126
HPC/KCl/polyaniline	Thermo/electrochromic dual response	73.0	57.5	30.0	127
PNIPAM/upconverting nanoparticles	Converting infrared light into visible light	82.8	79.8	40.0	128
PNIPAM/Si/Al	Printable hydrogel	80.1	72.7	35.0	129

 This journal is © The Royal Society of Chemistry 2024

Published on 25 April 2024. Downloaded by Yunnan University on 8/6/2025 12:09:49 AM.

2.2.4.1 Modulation of τ_c. The critical temperatures of thermochromic hydrogels need to be tunable to meet the requirement of different climates.[130] Some effective strategies, for example, introducing inorganic salts[122] and hydrophilic monomers,[23] have been demonstrated to modulate τ_c through suppressing phase separation of thermochromic hydrogels.

Inorganic salts are introduced into hydrogel networks to regulate phase transition temperature of thermochromic hydrogels. A thermochromic hydrogel-based smart window with good optical properties (T_{lum} of 99.1% and a ΔT_{sol} of 33.4%) is developed by copolymerizing hydrophilic acrylamide (AAM), hydrophobic stearyl methacrylate (C_{18}), and sodium dodecyl sulfate (SDS) micelles.[121] SDS micelles serve as surfactants to modulate the self-assembled particle size of the hydrophobic C_{18} phase that is covalently linked to PAAM chains, which influence the light transmittance and the phase transition temperature. The metal ions interact with the SDS headgroup ($-SO_4^-$) and reduce the electrostatic repulsion, leading to a lower critical micelle concentration (CMC) of SDS. The salt concentration and cation radius also affect the CMC of SDS. Thus, the thermochromic hydrogel presents a tunable phase transition temperature from 20 °C to 50 °C. Similarly, Tian *et al.* developed a PNIPAM hydrogel-based smart window with optical properties (T_{lum} of 92.7% and a ΔT_{sol} of 93.6%).[122] Adjustable phase transition temperature within 24.5–31.7 °C is achieved by changing the sodium chloride (NaCl) concentration. Na^+ interacts with the polymer surface and weakens the hydrogen bonds between amide groups of polymer chains and water. Thus, the phase separation of PNIPAM is more susceptible to the salt concentration, resulting in a tunable τ_c.

2.2.4.2 Solar modulation. Many thermochromic hydrogels have weak solar regulation capability. For example, pure PNIPAM hydrogels only possess a ΔT_{sol} of 25.5% at 52 μm thickness,[100] which limits the overall solar modulation performance of PNIPAM-based smart windows.[15,131] Many endeavors to improve light scattering performance have been made to enhance the modulation by introducing organic solvents,[123] incorporating inorganic nanoparticles,[124,132,133] developing chain/microparticle hybrid liquid smart windows,[112] *etc.*

Ding *et al.* constructed a PNIPAM hydrogel-based smart window through introducing ethanol to enhance solar modulation to 71.8%.[123] Ethanol decreases the size of scattering centers and increases the scattering center number. Meanwhile, it weakens interactions between water and polymer chains and discharges more water from the PNIPAM network during the phase transition, resulting in a high refractive index difference between PNIPAM and water. Thus, the hydrogel has highlight scattering behavior and presents an enhanced solar modulation ability.

W-doped VO_2 nanoparticles are introduced into PNIPAM/HPC hydrogels to enhance ΔT_{sol}.[124] W-doped VO_2 nanoparticles are attached to the surface and interior of PNIPAM/HPC hydrogels. As a result, the hydrogel presents a thicker pore wall and higher porous density, which scatters light above its τ_c, leading to a higher solar modulation ability of 65.7%.

A liquid hydrogel-based smart window is recently developed by copolymerizing *N*-isopropylacrylamide (NIPAM) and acrylic acid (AA).[112] The liquid hydrogel includes linear PNIPAM-PAA chains and Cu_3Cit_2@PNIPAM-PAA core–shell microgel particles. Above τ_c, the chains are dissolved and aggregate to form new compact microgel core–shell particles, which undergo a phase transition and shrink. The optical contrast between microgel particles and water results in strong light scattering performance, leading to an enhanced solar modulation ability. The synergetic effect of polymer chains-microgel particle conversion and core–shell particle shrinkage strengthens ΔT_{sol} to 85.5%.

2.2.4.3 Mechanical strength. Good mechanical properties of thermochromic materials are conducive to improving the service life of smart windows. Conventional thermochromic hydrogels usually have poor mechanical strength due to shrinkage and rupture of networks during the phase transition.[134–137] Many strategies based on ionic interactions,[117] double networks,[138] supramolecular assembly,[116] hydrogen bonding,[115] *etc.*, have been developed to improve the strength, toughness, and self-healing of thermochromic hydrogels.

Dai *et al.* developed a physically crosslinked ionogel by photopolymerizing hydroxyethyl acrylate (HEA) and butyl acrylate (BA) within ionic liquid $[BMIm]^+[BF_4]^-$ (Fig. 11a).[117] HEA and BA show excellent solubility in $[BMIm]^+[BF_4]^-$. The ionogel with three-dimensional porous structures has high-density molecular entanglements and cross-linking. The maximum fracture strain increases with the $[BMIm]^+[BF_4]^-$ content. Thus, the ionogel presents a tensile strength of 89.5 kPa at 670% fracture strain.

Zheng *et al.* reported a double-network hydrogel by incorporating PNIPAM-PAA microgels into a PAAM matrix for thermochromic smart windows, forming interpenetrating networks.[138] PNIPAM-PAA microgels prevent crack propagation, and the PAAM matrix serves as a sacrificial network to dissipate energy (Fig. 11b). As a result, the hydrogel with only 2 wt% microgels shows a fracture strength of around 70 kPa and breaking elongation of 420%.

An alcogel with supramolecular configuration is constructed to improve mechanical properties of smart windows.[116] The alcogel with 68.7 wt% ethanol content has host-cellulose chains wrapping guest-polyacrylamide (PAAM) chains through extensive hydrogen bonds. The alcogel shows compact supramolecular structures between cellulose and PAAM and ethanol-induced curling of PAAM chains. It shows a tensile strength of 13.6 MPa and a higher impact resistance of 42.8 kJ m^{-2} than ordinary glass (4.1 kJ m^{-2}) (Fig. 11c).

Li *et al.* fabricated a poly(propylene glycol) (PPG)-based ionogel by synthesizing hydroxyl-terminated PPG, isophorone diisocyanate (IPDI), and adipic acid dihydrazide (ADH) for thermochromic smart windows.[115] The hydrazide groups of ADH react with isocyanate groups to produce acylsemicarbazide (ASCZ) moieties. Meanwhile, multiple hydrogen bonds form between the ASCZ moieties, which increase the crosslinking density of the polymer network. Thus, the ionogel presents a high tensile strength of 5.58 MPa and a tensile strain of 3210%.

Published on 25 April 2024. Downloaded by Yunnan University on 8/6/2025 12:09:49 AM.

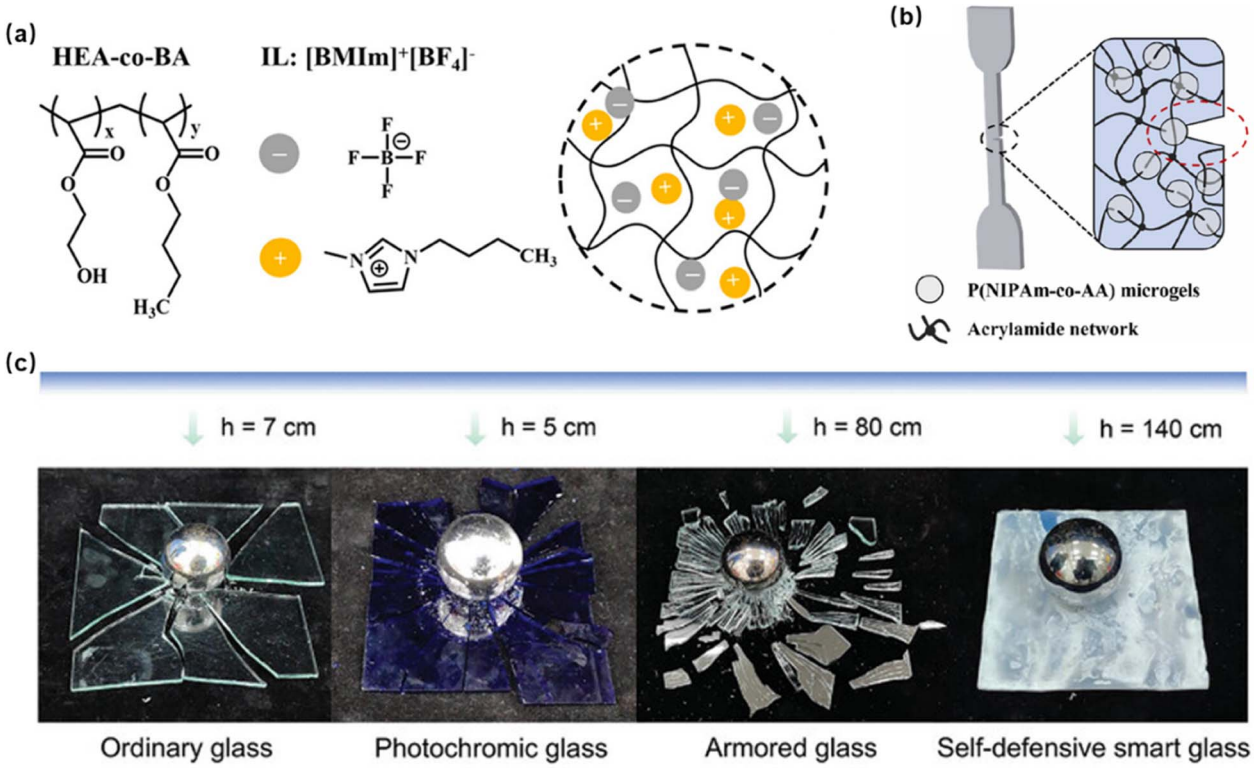

Fig. 11 (a) Schematic diagram of the ionogel network structure. Reproduced with permission from Dai *et al.*, ACS Appl. Polym. Mater. 5, 3398 (2023). Copyright 2023 American Chemical Society.[117] (b) Schematics of the PNIPAM-PAA/PAAM hydrogel with a crack under tension. Reproduced with permission from Zheng *et al.*, Compos. Commun. 42, 101684 (2023). Copyright 2023 Elsevier, Inc.[138] (c) Impact resistance testing of ordinary glass, photochromic glass, armored glass, and smart glass. Reproduced with permission from Chen *et al.*, Adv. Funct. Mater. 33, 2214382 (2023). Copyright 2023 Wiley-VCH GmbH.[116]

2.2.4.4 Antifreezing. Thermochromic anti-freezing hydrogels are required for smart windows in cold regions.[93,139] Recently, several strategies based on hydrogen bonding competition between polymer chains and water have been proposed to improve the anti-freezing ability of thermochromic hydrogels, including the introduction of organic solvents[118,125] and modulation of polymer structures.[95]

Wang *et al.* prepared an anti-freezing smart window with a T_{lum} of 89.3% and ΔT_{sol} of 80.7% by using thermochromic poly(*N*-isopropylacrylamide)-poly(*N*,*N*-dimethylacrylamide)/ethylene glycol hydrogel (PNIPAM-PDMAA/EG) that is resistant to low temperatures.[125] The introduction of EG is conducive to the formation more hydrogen bonds between polymer chains and water, which effectively hampers the freezing of the hydrogel. The hydrogel does not freeze at temperatures down to −100 °C. Similarly, an anti-freezing smart window with a T_{lum} of 90% and ΔT_{sol} of 60.8% is fabricated based on the noncovalent crosslinked PNIPAM hydrogel.[118] The PNIPAM hydrogel with a freezing point of around −18 °C is synthesized in a glycerol–water (GW) binary solvent system. The hydrogen bonds between glycerol and water are more stable than that between water and water, thereby resulting in excellent low-temperature resistance.

Feng *et al.* developed an anti-freezing hydrogel for smart windows with a T_{lum} of 80.7% and ΔT_{sol} of 64.5% by simply entangling PNIPAM and HPC together without adding other organic solvents.[95] The HPC fibers are liable to form hydrogen bonds with water, efficiently restricting water crystallization. As a result, the PNIPAM/HPC hydrogel has a good low-temperature resistant ability at −13 °C.

2.2.5 Thermochromic hydrogel smart windows for all climate solar modulation. Most thermochromic smart windows are triggered by high temperature in hot climates to block excessive solar radiation into buildings, which are usually applicable in low latitude areas in the summer. In order to extend the application spectrum of smart windows and improve their energy saving capability, it is desirable to develop smart windows suitable for different climates, particularly in cold weather in the winter. The capability to block heat radiation from buildings to outdoors is of special interest to keep buildings warm and save heating energy in winter. To achieve this, it is critical to develop thermochromic hydrogels with different transition temperatures over a broad range that adapt to different climates.

Dai *et al.* developed a thermochromic hydrogel with a reversible three-stage transition of opaque-transparent-translucent by introducing SDS and NaCl into the cross-linking network of PNIPAM-PAAM.[140] The solubility of SDS increases as the temperature increases and shows a clear transition point (Krafft point, T_k). At the temperature below T_k, SDS molecules separate from the solvent and precipitate inside the

 This journal is © The Royal Society of Chemistry 2024

Published on 25 April 2024. Downloaded by Yunnan University on 8/6/2025 12:09:49 AM.

hydrogel network, making the hydrogel opaque. At the temperature between T_k and τ_c, SDS micelles are formed and the hydrogel becomes transparent, which results in a T_{lum} of 80.3%. At temperature above τ_c, PNIPAM chains aggregate and form phase separated microdomains to scatter incident light. Thus, the hydrogel becomes opaque to inhibit indoor heat dissipation through the window to the outside at low temperature and demonstrates a ΔT_{sol} of 72.9%. Meanwhile, it becomes translucent to scatter sunlight at high temperature, showing a ΔT_{sol} of 42.7%. A model styrofoam house with a hydrogel smart window is used for the solar energy shielding test. The model house with normal glass is set as a control. The indoor temperature of the model house with a smart window is reduced by 3.6 °C after 30 minutes of infrared irradiation (55 °C), and the interior temperature of the model house with normal glass is 1.3 °C lower than that of the model house with a smart window after being placed in a cold closet for 40 minutes.

Recently, our group developed thermochromic hydrogel smart windows for all climate applications to modulate solar radiation and heat radiation.[23] The smart windows are equipped with LCST type thermoresponsive hydrogels with different τ_c. Transparent thermochromic hydrogels are prepared by copolymerizing hydrophilic *N*,*N*-dimethylacrylamide (DMAA) and NIPAM monomers at room temperature with UV initiation. The introduction of a hydrophilic DMAA monomer enhances hydrophilicity and then slightly suppresses phase separation at high temperatures. As a result, the LCST or τ_c of hydrogels gradually increases from 32.5 °C to 43.5 °C with increasing DMAA content in the network. Here, UV-initiated free radical polymerization at low temperature is used to avoid potential phase separation caused by reaction heat. The obtained hydrogels are highly transparent, with a luminous transmittance of 91.3%. In August, in Guangzhou, as an example, after 1 h of sunlight exposure at 14:00 p.m., the hydrogel smart window becomes opaque (Fig. 12a).

Two-compartment thermal insulation boxes are assembled to test the solar regulation ability of the smart windows in various climates. The test room is equipped with a thermochromic hydrogel smart window, and the control room is equipped with an ordinary double layer glass window (Fig. 12b). Here, the smart window comprises a thermochromic hydrogel sandwiched between two glasses. Since the refractive constant of the hydrogel is close to that of glass, the transmittance of smart windows is augmented from 79.4% to 85.5%. At high temperatures, the smart windows become opaque and prevent local heating. Therefore, the temperature of the test room is more uniform than that of the control room (Fig. 12c). The temperature increase of the test room (40.6–44.0 °C) is less than that of the control room (45.8–51.6 °C).

The smart windows show outstanding solar and heat modulation in different climates. Simulation tests are carried out in six cities (Beijing, Dalian, Xi'an, Shanghai, Fuzhou and Guangzhou) with different geographical locations and climates from December 2021 to August 2022 (Fig. 12d). In Guangzhou, a tropical southern city, the temperature in direct sunlight areas in the summer can reach 50–60 °C. The hydrogel smart window with a τ_c of 40.3 °C becomes opaque and scatters sunlight, showing a ΔT_{sol} of 88.8%. As a result, the air temperature in the test room (T_1) is lower than that in the control room (T_2). The indoor temperature is reduced by 4 °C in March, and an energy saving of 5.14 kJ m^{-3} is achieved (Fig. 12e). In December, in Dalian, the northern city, the ambient temperature in winter is below the freezing point and central heating temperature is used. As the room temperature is raised to 35 °C as a proof-of-concept test, the transparent hydrogel smart window with a τ_c of 33 °C becomes opaque and prevents indoor heat dissipation through the window to the outside. The temperature outside the test room (T_1) is 4.7 °C lower than that of the control room (T_2), and an energy saving of 6.05 kJ m^{-3} is achieved (Fig. 12f). These results demonstrate the capability of such smart windows to keep rooms "warm in winter and cool in summer".

On the other hand, the energy saving performance of smart windows is investigated by theoretical calculations based on theoretical models.[141] For example, Long *et al.* reported a thermochromic smart window using a HPC entangled PNIPAM hydrogel with a fiber structure.[95] At 20 °C, the fibers are thin and elongated to allow light to pass through, leading to a T_{lum} of 80.7%. In contrast, the fibers aggregate to scatter light at 40 °C, and thus the smart window shows a ΔT_{sol} of 64.5%. The energy consumption is calculated by using an actual-size house model (8 m in length, 6 m in width, and 2.7 m in height) with four windows (3 m in width and 2 m in height) and the weather conditions in Singapore. The calculation results show an energy saving of ~6 MJ m^{-2} in July. Moreover, the same group estimated the energy saving of another thermochromic smart window with a T_{lum} of 90% and ΔT_{sol} of 68.1% based on PNIPAM particle dispersion in water.[21] Such a smart window combines solar heat absorption by water with large specific heat capacity (4.2 kJ kg^{-1} K^{-1}) and the solar modulation of PNIPAM particles at 32 °C, which results in an energy saving of ~7 MJ m^{-2} in July. These results indicate that thermochromic smart windows are promising for building energy saving.

Such thermochromic hydrogel smart windows can be processed into well-designed structures to balance visibility and solar regulation. Gridded thermochromic hydrogel smart windows are prepared by 3D printing. Upon heating, the hydrogel grids become opaque, while the rest of the domains remain transparent. By adjusting the mesh size and density, both good visibility and solar modulation ability (59.6%) are achieved (Fig. 12g).

2.3 Other thermochromic materials

2.3.1 Ionic liquids. Ionic liquids (ILs) are regarded as non-volatile liquids and salts that consist of organic cations and anions.[142,143] ILs have no leakage or combustion problems and have been widely investigated and applied.[144–146] Meanwhile, ionic liquids have intrinsic thermochromic response behavior and are considered competitive candidates for smart windows (Fig. 13a).[147] When the temperature is below critical temperature, thermochromic ionic liquids adopt an octahedral configuration, which can change into tetrahedra as temperature

Published on 25 April 2024. Downloaded by Yunnan University on 8/6/2025 12:09:49 AM.

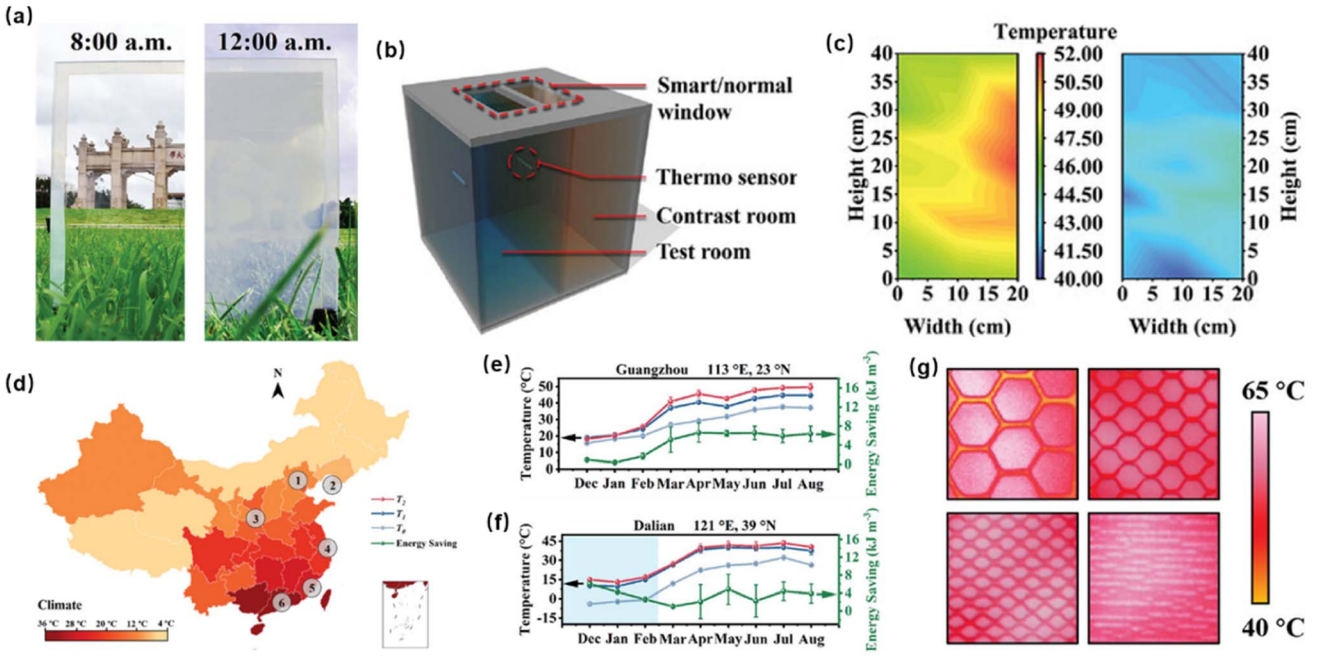

Fig. 12 Smart windows for all-climate applications. (a) Photos of a hydrogel smart window in the sun in Guangzhou. (b) Schematic illustration of a two-compartment simulation test setup. (c) Temperature distribution in the setup in the sun in Guangzhou, left: control and right: test group. (d) Field testing of hydrogel smart windows in Beijing, Xi'an, Shanghai, Fuzhou, Guangzhou and Dalian. Monthly temperature regulation and energy saving of smart windows in (e) Guangzhou and (f) Dalian, and temperature differences between test and control rooms, where T_0, T_1, and T_2 are temperatures in the shadow of the test group and the control group. (g) Thermal infrared images of hydrogel smart windows with different grid patterns. Reproduced with permission from Chen *et al.*, Adv. Mater. 35, 2211716 (2023). Copyright 2023 Wiley-VCH GmbH.[23]

exceeds the critical transition temperature, resulting in a significant light transmittance variation.[12]

Ionic liquids can be used to prepare thermochromic ionogels for use in smart windows. For example, Wu *et al.* reported a thermochromic ionic liquid-based gel electrolyte with a T_{lum} of 90.2% and ΔT_{sol} of 82.3% for thermos-/electro-dual-responsive smart windows.[148] With the addition of an ionic liquid, hydrogen bonds form between the polymer network and ionic liquid, which result in better swelling and movement of polymer segments, leading to an adjustable τ_c (47–55 °C).

Combining thermochromic ionic liquid-based gels with other mechanisms can impart multiple adjustabilities to smart windows. A thermochromic ionic liquid 1-ethyl-3-methylimidazolium bis(trifluoromethylsulfonyl)imide ([EMIM]TFSI) microemulsion-based gel is prepared by polymerizing an acrylamide monomer in an ionic liquid-based microemulsion.[149] Tween 20 is distributed at the oil–water interface to stabilize the droplets in the ionic liquid microemulsion. At 25 °C, the droplets are stable and difficult to precipitate. Thus, the thermochromic gel shows a T_{lum} of 99.3%. When temperature is above 40 °C, the microemulsion droplets aggregate, which highly scatter the incident light, leading to a high ΔT_{sol} of 92.6%. Besides, [EMIM]TFSI endows the thermochromic gel with ionic conductivity. Thus, the gel is also utilized as an electrolyte layer for electrochromic smart windows. Integrating the conductive gel with a WO_3 electrochromic layer achieves electric-/thermal-dual modulation of smart windows. Similarly, Deng *et al.* constructed a thermochromic ionic liquid 1-butyl-3-methylimidazolium tetrafluoroborate ($BMIMBF_4$)-based gel electrolyte by polymerizing *N*-isopropylacrylamide.[150] At temperature below LCST, the PNIPAM chains are dissolved in $BMIMBF_4$ and water. When temperature is above LCST, the polymer chains aggregate into globules to scatter incident light, leading to a good thermochromic performance. Moreover, $BMIMBF_4$ endows the gel with ionic conductivity up to 15.4 mS cm^{-1}. Combining the thermochromic PNIPAM layer with an electrochromic TiO_2 layer, an electric-/thermal-dual smart window is developed.

2.3.2 Perovskites. Perovskites are a class of materials with significant optoelectronic performances and scalable manufacturing processibility.[151–153] Thermochromic perovskites have a reversible color switch in response to temperature changes without additional energy input and are thus recognized as ideal candidate materials for smart windows.[154,155] Thermochromic perovskites have thousands of complex constructures, mainly including three-dimensional (3D), two-dimensional (2D), one-dimensional (1D), zero-dimensional (0D), double perovskite forms, *etc.* Among them, 3D perovskites are the focus of research. Metal halide perovskites with structure ABX_3 [A and B are the larger and smaller cations respectively and X represents the anion] are widely used in smart windows.[156–158]

The thermochromic mechanism of perovskites is based on its abnormal crystallization phenomenon that its solubility gradually decreases with an increase in temperature. At low temperature, the solubility of thermochromic perovskites is

 This journal is © The Royal Society of Chemistry 2024

Published on 25 April 2024. Downloaded by Yunnan University on 8/6/2025 12:09:49 AM.

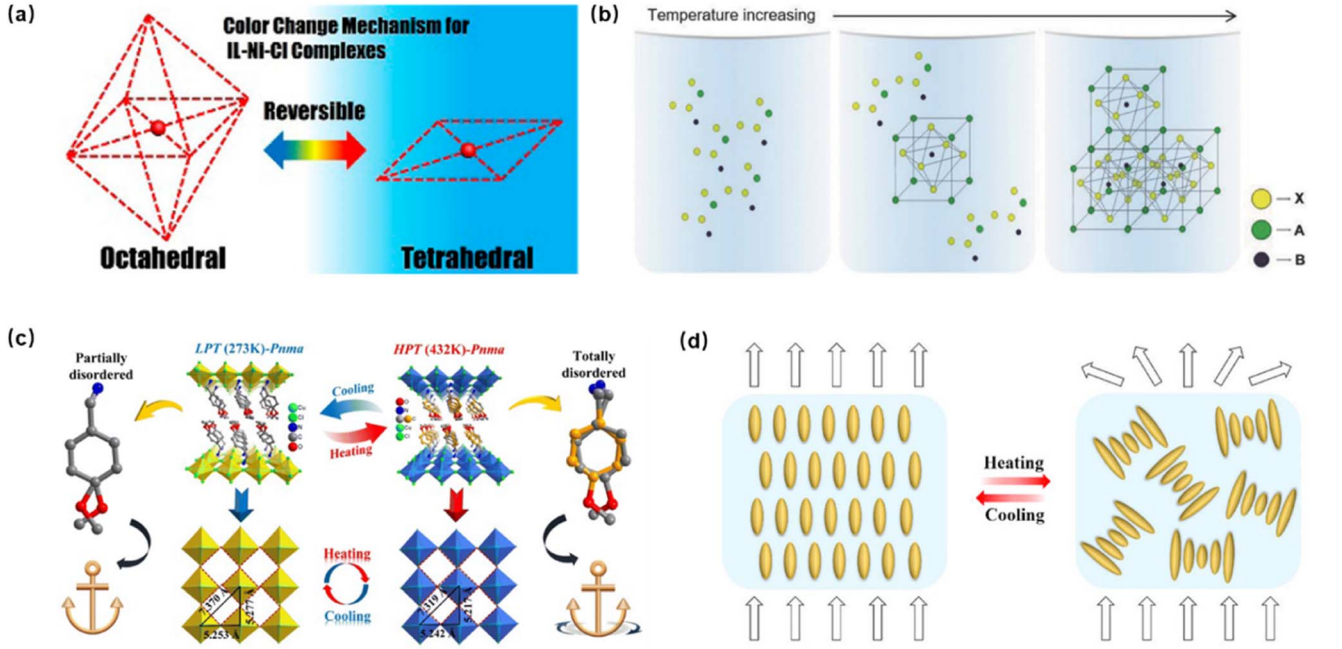

Fig. 13 (a) The temperature-dependent crystal structure change of ionic liquids. Reproduced with permission from Zhu *et al.*, ACS Appl. Mater. Interfaces 8, 29742 (2016), Copyright 2016 American Chemical Society.[147] (b) Schematic illustration of the change process of perovskite materials: with increasing temperature, the perovskite crystals nucleate and grow. Reproduced with permission from Ke *et al.*, Adv. Funct. Mater. 28, 1800113 (2018). Copyright 2018 Wiley-VCH GmbH.[12] (c) Schematic diagram of the structures in a hybrid perovskite compound. Reproduced with permission from Teri *et al.*, J. Mater. Chem. C 11, 8903 (2023). Copyright 2023 Royal Society of Chemistry.[160] (d) Schematic illustration of the phase transition between the aligned phase and focal conic phase. Reproduced with permission from Shen *et al.*, Laser Photonics Rev. 17, 2200207 (2023). Copyright 2023 Wiley-VCH GmbH.[167]

high, and the hydrated perovskite is colorless to allow sunlight to pass through. As the temperature increases, the solubility of the perovskite decreases, and the colorless perovskite hydrate phase transforms into a colored photovoltaic perovskite phase to block sunlight (Fig. 13b).[12,159]

Thermochromic perovskites show a red shift in absorbance with increasing temperature. Teri *et al.* developed a copper-based hybrid perovskite $(MBA)_2CuCl_4$ (MBA is 4-methoxybenzylamine) with a reversible phase transition temperature of 430.2 K.[160] The dielectric states are different because the organic aminium cations transition between partial order and disorder states (Fig. 13c). The coordinate geometry of Cu^{2+} is relevant with the position of the absorption maximum for the d–d transition. The structure of Cu-based perovskite changes from tetrahedral coordination to an octahedron with increasing temperature, which causes a shift in the electronic absorption band. Thus, the red shift of hydride perovskite occurs in the absorbance spectrum, resulting in a color change from yellow to brown.

One challenge of perovskite-based smart windows is how to reduce the high critical transition temperature to around ambient temperature. Liu *et al.* fabricated a novel smart window based on the thermochromic perovskite H-$MAPbI_{3-}Cl_x$ with a ΔT_{sol} of 23.7%.[161] The hydration and dehydration processes of thermochromic perovskite H-$MAPbI_{3-x}Cl_x$ during the phase transition demonstrate that the ambient humidity is important to the τ_c. When the relative humidity decreases to 50%, the τ_c is around 40 °C, which is lower than that of 80% relative humidity (51.4 °C). The τ_c can be reduced from 51.4 °C to 29.4 °C with a decrease in relative humidity (from 80% to 25%).

Developing alternative strategies to trigger the thermochromic effect of perovskite-based smart windows at ambient temperatures is necessary for applications. Liu *et al.* proposed a NIR activated perovskite-based smart window at room temperature.[154] The smart window is fabricated by integrating cesium-doped tungsten trioxide (CWO) with T-perovskite H-$MAPbI_{3-x}Cl_x$. CWO has high visible transmittance of 82% and strong NIR absorption of 90%. As a result, the perovskite-based smart window shows a T_{lum} of 65.7%. At 23.5 °C, the strong NIR absorption of the CWO layer produces thermal energy and heats the window to the phase transition temperature of thermochromic perovskite. Then the thermochromic T-perovskite dissociates water from the $MAPbI_{3-x}Cl_x$ layer. Thus, the smart window changes from a transparent state to a colored state and shows a ΔT_{sol} of 17.5%.

2.3.3 Liquid crystals. Liquid crystals (LCs) are neutral organic compounds and regarded as the fourth state of matter. LCs typically present rodlike or disclike phases, which are anisotropic in optical, electrical, and magnetic properties.[162] The arrangement of mesogenic molecules can be regulated in response to an electrical field,[163] external temperature,[164] a magnetic field,[165] *etc.* Although liquid crystal smart windows driven by an electric field have been widely investigated and commercialized,[166] it is needed to develop next-generation

Published on 25 April 2024. Downloaded by Yunnan University on 8/6/2025 12:09:49 AM.

liquid crystal smart windows with high modulation capability and free of energy input (*e.g.*, an electric field).[167] Thermochromic liquid crystals have been recently reported to change molecular orientation upon temperature changes.[168–170] Specifically, thermochromic liquid crystals show perpendicularly aligned smectic A (SmA) phases at low temperatures and will undergo phase transitions to chiral nematic (N*) phases with focal-conic texture when the temperature is raised above the phase transition temperature. The phase transition temperature can be modulated in the range of 10–40 °C by adjusting the concentration of monomers.[171,172] The temperature-induced phase transition is accompanied by changes in molecular orientation and optical states (Fig. 13d).[167] Thermochromic liquid crystals are composited with a polymer matrix to prepare thin film smart windows.[173,174] Liquid crystals are embedded in crosslinked polymer networks as droplets. The composites with liquid crystal molecules anchored in the polymer network usually experience reversible changes in the liquid crystal orientations, matching/mismatching in refractive indices,[170] and thus optical properties upon an external stimulus.[175]

Liquid crystal-based thermochromic smart windows have excellent solar modulation capability because their strong control in both visible and near-infrared regions. For example, Liang *et al.* developed a thermochromic liquid crystal-based film with a T_{lum} of 67%.[172] The composite film is composed of liquid crystal, poly(vinylpyrrolidone) (PVP), and tungsten bronze (Cs_xWO_3) nanorods. The phase of liquid crystal changes from a smectic state to a chiral nematic state with an increase in temperature, which provides a change from transparency to opaqueness. Cs_xWO_3 has strong and broadband LSPR absorption of NIR irradiation. Thus, the liquid crystal-based smart window shows an ultrahigh near-infrared irradiation shielding of 95% from 800 nm to 2500 nm.

Combining the thermochromic mechanism of liquid crystals with other mechanisms can give the smart windows multiple adjustment capabilities. Meng *et al.* constructed a photothermal dual-driven liquid crystal-based smart window.[176] When the ambient temperature is 26 °C, the liquid crystal presents a smectic phase, allowing incident light to pass through, resulting in a T_{lum} of 70%. When the ambient temperature is above 41 °C, the liquid crystal changes from the smectic phase to a cholesteric phase. Then the refractive index of the liquid crystal is changed in the thickness direction. Therefore, the liquid crystal-based smart window scatters light, leading to 50% reduction in transmittance. Moreover, a photothermal molecule, isobutyl-substituted diimmonium borate (IDI), is doped into the liquid crystal-based system. IDI has strong absorption in the NIR range, and the temperature of the liquid crystal-based system with IDI increases from 24 °C to about 31.7 °C under sunlight for 160 seconds. IDI can convert light irradiation to heat and accelerate the phase change of the liquid crystal, leading to a photothermal dual-driven smart window. Similarly, an electrical/thermal dual-control film with 57.8% T_{lum} and 34.6% ΔT_{sol} is prepared by combining liquid crystal/polyacrylate with W-doped VO_2.[177] The composite materials are sandwiched between two plastic conductive substrates. At low environmental temperature and no voltage, the composite materials present a homeotropically aligned liquid-crystalline polymer network. Both the liquid crystal and polymer possess similar refractive indices so that the film appears transparent. When an electric field is applied, the liquid crystal domains are aligned parallel across the direction of the electric field, yielding an anisotropic distribution of refractive index values. The difference between the liquid crystal and polymer results in light scattering. Meanwhile, the thermochromic W-doped VO_2 exhibits passively thermochromic behavior during the phase transition at 43.2 °C. Thus, the liquid crystal-based composite materials are promising for smart windows that can be activated by temperature changes and/or using an electric field.

3. Thermoelectricity conversion and solar cells

The current philosophy of thermochromic smart windows discards reflected solar energy.[27,178,179] To further improve the energy saving efficiency, it is necessary to harness blocked solar energy. Many studies have been reported to achieve simultaneous modulation and utilization of solar radiation with smart windows. For example, solar thermoelectricity materials and devices can produce electrical potential during temperature changes.[180–182] Moreover, integrating solar cells with thermochromic materials can boost the generation of new smart windows that can not only modulate solar radiation, but also generate electricity through direct solar-electrical conversion.[183,184]

3.1 Thermoelectricity conversion

Thermoelectricity conversion is considered a clean photovoltaic technology based on the Seebeck effect,[185,186] which usually converts temperature variations induced by the solar-thermal conversion effect into electricity by using a solar thermoelectric generator.[187] For example, Zhang *et al.* prepared a phase change composite with polybenzobisoxazole fibers through a molding process.[179] The fibrous crystals in fibers offer thermal pathways during the charging/discharging processes (Fig. 14a). The unique actinomorphic structure facilitates a controllable thermo-conductive performance and promises a good match with the charging rate to convert solar thermal energy into electricity. As a result, the solar thermoelectric generator shows an output voltage of 3.41 V and a power density of 198.7 W m^{-2}.

Although the solar thermal-electric conversion ability has been improved, it is still rare to design thermal-electric conversion smart windows due to high operation temperature and low visible transmittance. Zhang *et al.* constructed a $Cs_{0.33}WO_3$/resin/glass smart window with a high luminous transmittance of 88% and outstanding solar absorption (Fig. 14b).[28] The absorbed near-infrared light and ultraviolet light can be effectively converted into heat. The thermoelectric system attached to the edges of the film collects the heat and transforms it into electricity. The smart window shows an output voltage of around 4 V. Besides, under a sunlight intensity of 100 mW cm^{-2}, the open-circuit voltage and maximum power

 This journal is © The Royal Society of Chemistry 2024

Published on 25 April 2024. Downloaded by Yunnan University on 8/6/2025 12:09:49 AM.

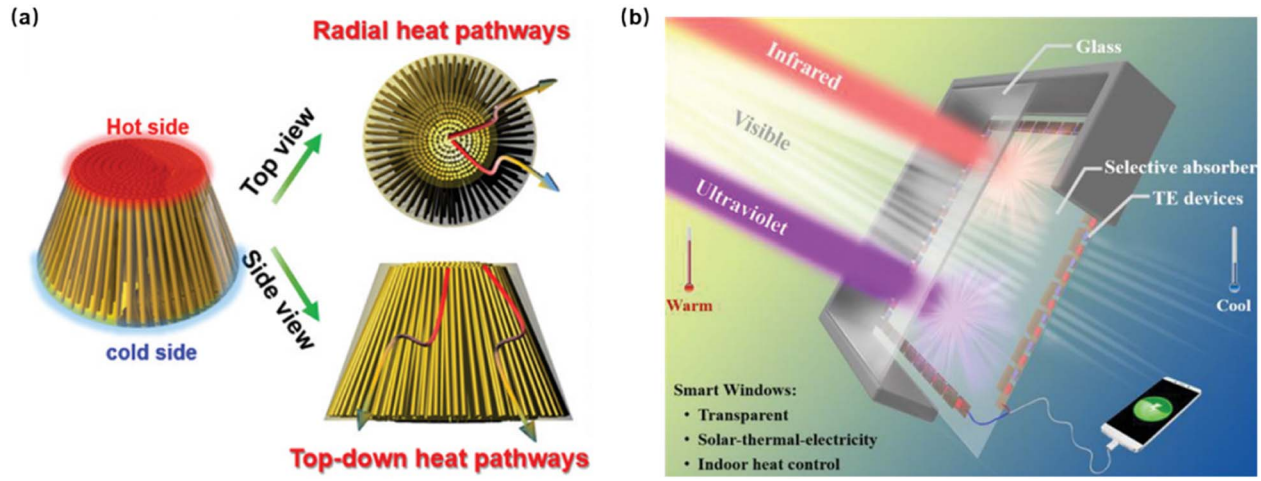

Fig. 14 (a) Schematic for multi-directional heat conduction in the phase change composite. Reproduced with permission from Zhang *et al.*, Adv. Funct. Mater. 32, 2109255 (2022). Copyright 2022 Wiley-VCH GmbH.[179] (b) Schematic illustration of the proposed power-generating smart window architecture and working process. Reproduced with permission from Zhang *et al.*, Adv. Energy Mater. 11, 2101213 (2021). Copyright 2021 Wiley-VCH GmbH.[28]

density reach up to 3.8 V and 0.4 mW cm^{-2} respectively. This work not only realizes efficient energy saving and power generation in the field of smart windows, but also provides significant insights and promising pathways for building energy saving.

3.2 Integration with solar cells

Integrating thermochromic materials with solar cells is an effective way to achieve thermochromic modulation and power generation.[188,189] It has been demonstrated that combining thermochromic VO_2-based materials with solar cells can simultaneously realize light harvesting and modulation. For example, Guo *et al.* constructed a photovoltaic smart window through combing a thermochromic VO_2 layer and an organic solar cell.[188] The VO_2 layer can intelligently modulate near-infrared light according to the environmental temperature. The organic solar cell can convert visible light into electricity. Therefore, the VO_2-based smart window shows a luminous transmittance of 28.2%, a solar modulation ability of 7.5%, and a power generation efficiency of 3.1%. This work pioneers a research direction for designing electrical-generating smart windows, but the thermochromic properties and electrical generation efficiency of smart windows are limited. Meng *et al.* prepared a photovoltaic smart window by integrating W-doped VO_2 nanoparticles and organic perovskites.[190] As shown in Fig. 15a, the smart window presents not only high visible transmittance at both high and low temperatures, but also a strong solar modulation capability of 10.7% due to the phase transition behavior of thermochromic W-doped VO_2. A low-E coating is placed on the surface of glass to enhance the thermal insulation. The electron transport layer between thermochromic W-doped VO_2 and perovskite promotes extraction and transport of photogenerated charges. As a result, the smart device exhibits a high-power conversion efficiency of 15.4% at 25 °C and 16.1% at 45 °C.

Thermochromic hydrogels have also been widely combined with solar cells to achieve both energy saving and energy

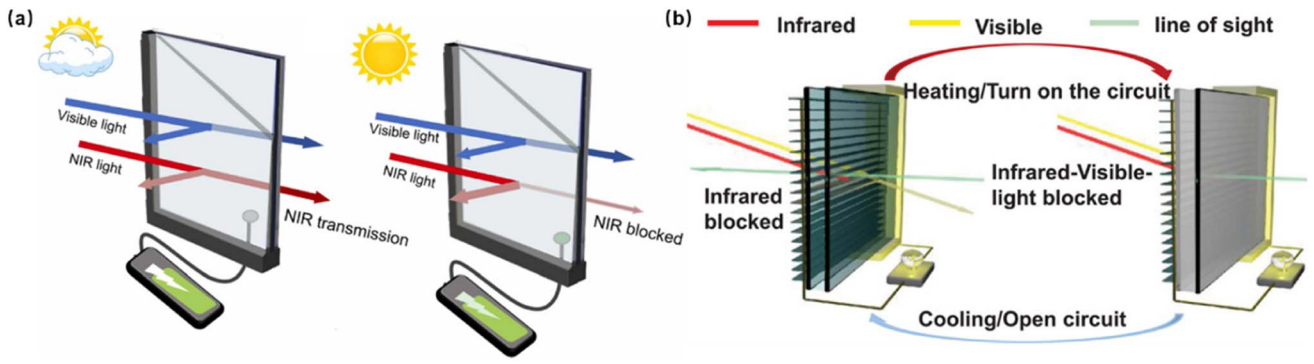

Fig. 15 (a) Illustration of the photovoltaic smart window work on cold and warm days. Reproduced with permission from Meng *et al.*, Nano Energy 91, 106632 (2022). Copyright 2022 Elsevier, Inc.[190] (b) The schematic diagram of the energy saving and energy storage integrated smart window in different environments. Reproduced with permission from Niu *et al.*, Adv. Sci. 9, 2105184 (2022). Copyright 2022 Wiley-VCH GmbH.[191]

Published on 25 April 2024. Downloaded by Yunnan University on 8/6/2025 12:09:49 AM.

generation. For example, Niu *et al.* constructed a multi-layer louver smart window containing a thermochromic host–guest hydrogel (HGT hydrogel) and Si-based solar cell (Fig. 15b).[191] The HGT hydrogel is prepared by introducing HPC microparticles into the transparent PAM-PAA hydrogel matrix. Solar light can pass through the smart window at low temperatures, but the incident light is blocked due to the microstructure change of the HGT hydrogel at high temperatures. Therefore, the louver smart window has an ultrahigh luminous transmittance of around 90% and a strong solar modulation capability of about 54%. The unique louver structure of solar cell endows the smart window with an outstanding energy generation capability of 18.2%. Besides, the louver smart window exhibits a lower temperature of 13.3 °C than the normal one after 1 h radiation of simulated sunlight, showing good energy-saving performance. Similarly, Meng *et al.* developed a photovoltaic smart window by integrating a thermochromic HPC hydrogel with a perovskite solar cell.[192] Because of the structural transition of the HPC hydrogel, the photovoltaic smart window has a luminous transmittance of 27.3% at 20 °C and 10.4% at above 40 °C, as well as a solar modulation ability of 15.7%. Indium tin oxide is used as the electrode of the solar cell. The smart window presents a high peak conversion efficiency of 17.5%. An excellent combination of solar modulation and power generation is achieved in this smart window, contributing to sustainable building energy saving.

4. Conclusion and outlook

Thermochromic smart windows have received increasing attention for applications in building energy saving. In this review, we have summarized the recent progress of high performance smart windows based on thermochromic materials from response mechanisms and improved strategies for energy-saving applications. Emerging thermochromic smart windows can convert reflected solar energy into electricity through thermoelectricity conversion or solar cell technology.

Despite many excellent properties of thermochromic smart windows, there are still many challenges and unmet demands that stimulate further studies in this field. More novel thermoresponsive materials should be explored to satisfy the expansive application range of smart windows. Besides, the performances of current thermochromic materials are unsatisfactory and need to be improved. For example, the undesired color, biotoxicity and instability of VO_2 severely restrict its development. And it is difficult to achieve a perfect balance of τ_c, ΔT_{sol} and T_{lum} in thermochromic VO_2. Thermochromic hydrogels have an outstanding solar modulation ability in smart windows based on their reversible hydrophilic/hydrophobic phase transition. However, the problems of solvent volatilization, freezing and mechanical weakness of hydrogels cannot be ignored. Then the high cost and intricate fabrication process of ionic liquids, perovskites and liquid crystals also need to be solved. Additionally, structural modification that elevates thermochromic performances have been successfully realized in VO_2 and hydrogel systems, and different thermosensitive materials typically possess different modulation ranges of solar light. Thus, more efforts should be devoted to structure modification and composite application of thermochromic materials.

Thermoelectricity conversion based on the Seebeck effect for thermochromic smart windows is rarely investigated. More investigations are needed to develop new materials and mechanisms to promote the development of building energy generation. For solar cell integration, the low light transmittance and undesired color state should be addressed. Solar cells in smart windows have a lower power conversion efficiency than traditional perovskite cells due to the limitation of the phase transition of thermochromic materials; hence more fundamental research on the photovoltaic properties of solar cells should be conducted to enhance the electricity generation of thermochromic smart windows.

There are still some challenges with thermochromic smart windows to be addressed to meet commercial use. Common thermochromic smart windows are fabricated by sandwiching thermosensitive materials between two pieces of normal glass. The additional expenditure for thermosensitive materials and encapsulation is huge. Besides, the thermochromic properties of thermosensitive materials weaken with time, and therefore smart windows need to be regularly maintained and repaired. The long-term service life of thermochromic smart windows is important in practical applications of building. To this end, thermosensitive materials should have stable structures and optical properties. Traditional thermochromic materials show slow response times due to the tardy phase transition process caused by outdoor temperature changes. Thus, photo-thermal nanoparticles or additional applied voltage should be introduced to the thermochromic intelligent system to accelerate the response process. To meet the practical requirements of active control or privacy protection, thermal response smart windows should be combined with other stimuli to realize dual-response or even multi-response smart windows. Moreover, the promising trend is to integrate other functions into smart windows, such as self-cleaning, water harvesting, energy storage, super hydrophobicity, anti-drying, anti-freezing, *etc.* On the one hand, it is necessary to optimize the solar modulation of smart windows while maintaining good luminous transmittance. On the other hand, combining smart windows with solar cells to collect solar radiation and convert it into electricity will further enhance building energy saving.

In the future, smart windows will become a meaningful platform. Artificial intelligence and 5G society emerge one after another with increasing sophistication, so that smart windows may be more intelligent with other amazing features to serve people, for example, danger warning, sound insulation, intelligent ventilation, film projection, weather forecasts, and so on. We expect that more research communities will devote efforts together to promote the development of smart windows because the smart window system is a highly interdisciplinary technique. Throughout future developments, thermochromic smart windows will face tremendous tasks and challenges, but in parallel, they will also offer the exciting prospect of building energy saving.

 This journal is © The Royal Society of Chemistry 2024

Published on 25 April 2024. Downloaded by Yunnan University on 8/6/2025 12:09:49 AM.

Conflicts of interest

There are no conflicts to declare.

Acknowledgements

The authors are indebted to financial support from the National Natural Science Foundation of China (22375225, J. F.) and Postgraduate Education Foundation of Sun Yat-sen University (29000-11230011, G. C.).

References

1 A. Balali, A. Yunusa-Kaltungo and R. Edwards, *Renew. Sustainable Energy Rev.*, 2023, **171**, 113013.
2 Y. D. Priore, G. Habert and T. Jusselme, *Energy Build.*, 2023, **278**, 112598.
3 X. Zhao, A. Aili, D. Zhao, D. Xu, X. Yin and R. Yang, *Cell Rep. Phys. Sci.*, 2022, **3**, 100853.
4 M. W. Akram, M. Hasannuzaman, E. Cuce and P. M. Cuce, *Energy Built Environ.*, 2023, **4**, 206–226.
5 D. Yu, S. Zhuo, J. Wang, Z. Liu, J. Ye, Y. Wang, L. Chen, X. Ouyang, K.-Q. Zhang, X.-Q. Zhou, J. Guan, Y. Liu, W. Chen, L.-S. Liao and M.-P. Zhuo, *Small*, 2023, **19**, 2205833.
6 K. Okimura, M. S. Mian, I. Yamaguchi and T. Tsuchiya, *Sol. Energy Mater. Sol. Cells*, 2023, **251**, 112162.
7 H. Zhang, F. Sun, J. Feng, H. Ling, D. Zhou, G. Cao, S. Wang, F. Su, Y. Tian and Y. Tian, *Cell Rep. Phys. Sci.*, 2022, **3**, 101193.
8 Y. Ke, Q. Zhang, T. Wang, S. Wang, N. Li, G. Lin, X. Liu, Z. Dai, J. Yan and J. Yin, *Nano Energy*, 2020, **73**, 104785.
9 Y. Zhou, F. Fan, Y. Liu, S. Zhao, Q. Xu, S. Wang, D. Luo and Y. Long, *Nano Energy*, 2021, **90**, 106613.
10 Y. Badour, S. Danto, S. Albakour, S. Mornet, N. Penin, L. Hirsch and M. Gaudon, *Sol. Energy Mater. Sol. Cells*, 2023, **255**, 112291.
11 J. Harada, M. Taira and K. Ogawa, *Cryst. Growth Des.*, 2017, **17**, 2682–2687.
12 Y. Ke, C. Zhou, Y. Zhou, S. Wang, S. H. Chan and Y. Long, *Adv. Funct. Mater.*, 2018, **28**, 1800113.
13 Y. Cui, Y. Ke, C. Liu, Z. Chen, N. Wang, L. Zhang, Y. Zhou, S. Wang, Y. Gao and Y. Long, *Joule*, 2018, **2**, 1707–1746.
14 Y. Ke, J. Chen, G. Lin, S. Wang, Y. Zhou, J. Yin, P. S. Lee and Y. Long, *Adv. Energy Mater.*, 2019, **9**, 1902066.
15 Z. Zhang, L. Zhang, Y. Zhou, Y. Cui, Z. Chen, Y. Liu, J. Li, Y. Long and Y. Gao, *Chem. Rev.*, 2023, **123**, 7025–7080.
16 X.-H. Li, C. Liu, S.-P. Feng and N. X. Fang, *Joule*, 2019, **3**, 290–302.
17 Q. Lei, L. Wang, H. Xie and W. Yu, *Build. Environ.*, 2022, **222**, 109407.
18 J. Pi, C.-B. Li, R.-Y. Sun, L.-Y. Li, F. Wang, F. Song, J.-M. Wu, X.-L. Wang and Y.-Z. Wang, *Compos. Commun.*, 2022, **32**, 101167.
19 P. Sirvent, A. Tanguy, G. Pérez, R. Charriere and J. Faucheu, *Adv. Eng. Mater.*, 2022, **24**, 2101547.
20 Y. Zhou, X. Dong, Y. Mi, F. Fan, Q. Xu, H. Zhao, S. Wang and Y. Long, *J. Mater. Chem. A*, 2020, **8**, 10007–10025.
21 Y. Zhou, S. Wang, J. Peng, Y. Tan, C. Li, F. Y. C. Boey and Y. Long, *Joule*, 2020, **4**, 2458–2474.
22 J. Guo, S. Wu, Y. Wang, J. Huang, H. Xie and S. Zhou, *Mater. Horiz.*, 2022, **9**, 3039–3047.
23 G. Chen, K. Wang, J. Yang, J. Huang, Z. Chen, J. Zheng, J. Wang, H. Yang, S. Li, Y. Miao, W. Wang, N. Zhu, X. Jiang, Y. Chen and J. Fu, *Adv. Mater.*, 2023, **35**, 2211716.
24 S. Wang, T. Jiang, Y. Meng, R. Yang, G. Tan and Y. Long, *Science*, 2021, **374**, 1501–1504.
25 K. Tang, K. Dong, J. Li, M. P. Gordon, F. G. Reichertz, H. Kim, Y. Rho, Q. Wang, C.-Y. Lin, C. P. Grigoropoulos, A. Javey, J. J. Urban, J. Yao, R. Levinson and J. Wu, *Science*, 2021, **374**, 1504–1509.
26 P. Yu, J. Liu, W. Zhang, Y. Zhao, Z. He, C. Ma, H. Zhang, Z. Miao and W. Shen, *Dyes Pigm.*, 2022, **208**, 110817.
27 S. Owusu-Nkwantabisah, J. Gillmor, S. Switalski, M. R. Mis, G. Bennett, R. Moody, B. Antalek, R. Gutierrez and G. Slater, *Macromolecules*, 2017, **50**, 3671–3679.
28 Q. Zhang, A. Huang, X. Ai, J. Liao, Q. Song, H. Reith, X. Cao, Y. Fang, G. Schierning, K. Nielsch, S. Bai and L. Chen, *Adv. Energy Mater.*, 2021, **11**, 2101213.
29 X. Cao, T. Chang, Z. Shao, F. Xu, H. Luo and P. Jin, *Matter*, 2020, **2**, 862–881.
30 S. Bhupathi, S. Wang, M. Abutoama, I. Balin, L. Wang, P. G. Kazansky, Y. Long and I. Abdulhalim, *ACS Appl. Mater. Interfaces*, 2020, **12**, 41905–41918.
31 C. Lin, J. Hur, C. Y. Chao, G. Liu, S. Yao, W. Li and B. Huang, *Sci. Adv.*, 2022, **8**, 7359.
32 Q. Cheng, S. Paradis, T. P. Bui and M. F. Almasri, *IEEE Sens. J.*, 2011, **11**, 167–175.
33 Y. Oka, T. Yao and N. Yamamoto, *J. Mater. Chem.*, 1991, **1**, 815–818.
34 L. Whittaker, C. J. Patridge and S. Banerjee, *J. Phys. Chem. Lett.*, 2011, **2**, 745–758.
35 M. W. Haverkort, Z. Hu, A. Tanaka, W. Reichelt, S. V. Streltsov, M. A. Korotin, V. I. Anisimov, H. H. Hsieh, H. J. Lin, C. T. Chen, D. I. Khomskii and L. H. Tjeng, *Phys. Rev. Lett.*, 2005, **95**, 196404.
36 A. S. Belozerov, M. A. Korotin, V. I. Anisimov and A. I. Poteryaev, *Phys. Rev. B: Condens. Matter Mater. Phys.*, 2012, **85**, 045109.
37 L. Y. Rui Sun, J. He and J. Liang, *Prog. Chem.*, 2019, **31**, 1712–1728.
38 A. Moatti, R. Sachan, J. Prater and J. Narayan, *ACS Appl. Mater. Interfaces*, 2017, **9**, 24298–24307.
39 D. Lee, B. Chung, Y. Shi, G.-Y. Kim, N. Campbell, F. Xue, K. Song, S.-Y. Choi, J. Podkaminer and T. Kim, *Science*, 2018, **362**, 1037–1040.
40 V. Eyert, *Phys. Rev. Lett.*, 2011, **107**, 016401.
41 O. Nájera, M. Civelli, V. Dobrosavljević and M. J. Rozenberg, *Phys. Rev. B: Condens. Matter Mater. Phys.*, 2018, **97**, 045108.
42 N. B. Aetukuri, A. X. Gray, M. Drouard, M. Cossale, L. Gao, A. H. Reid, R. Kukreja, H. Ohldag, C. A. Jenkins and E. Arenholz, *Nat. Phys.*, 2013, **9**, 661–666.

Published on 25 April 2024. Downloaded by Yunnan University on 8/6/2025 12:09:49 AM.

43 T. V. Slusar, J.-C. Cho, H.-R. Lee, J.-W. Kim, S. J. Yoo, J.-Y. Bigot, K.-J. Yee and H.-T. Kim, *Sci. Rep.*, 2017, **7**, 16038.
44 J. Wei, Z. Wang, W. Chen and D. H. Cobden, *Nat. Nanotechnol.*, 2009, **4**, 420–424.
45 M. Li, S. Magdassi, Y. Gao and Y. Long, *Small*, 2017, **13**, 1701147.
46 Z. Zou, Z. Zhang, J. Xu, G. Li, R. Xiong, Y. Liu and J. Shi, *J. Mater. Sci.: Mater. Electron.*, 2021, **32**, 23825–23833.
47 B. Li, S. Tian, Z. Wang, B. Liu, X. Gong and X. Zhao, *Appl. Surf. Sci.*, 2021, **568**, 150959.
48 Y. Zhan, Y. Lu, X. Xiao, J. Wang, Y. Liu, S. Zhang, C. Shen, X. Xu and G. Xu, *Ceram. Int.*, 2020, **46**, 2079–2085.
49 S. Long, X. Cao, N. Li, Y. Xin, G. Sun, T. Chang, S. Bao and P. Jin, *Sol. Energy Mater. Sol. Cells*, 2019, **189**, 138–148.
50 X. Yang and J. Zou, *J. Alloys Compd.*, 2023, **940**, 168868.
51 X. Zhao, J. Sun, Z. Guo, J. Su, T. Liu, R. Hu, W. Yao and X. Jiang, *Chem. Eng. J.*, 2022, **446**, 137308.
52 B. Zhuang, Z. Dai, S. Pang, H. Xu, L. Sun and F. Ma, *Adv. Opt. Mater.*, 2019, **7**, 1900600.
53 Q. Lu, C. Liu, N. Wang, S. Magdassi, D. Mandler and Y. Long, *J. Mater. Chem. C*, 2016, **4**, 8385–8391.
54 D. Zhou, H. Zong, Q. Hu, L. Yan, W. Qiao, S. Zhang, J. Pan, Z. Liu and M. Li, *Infrared Phys. Technol.*, 2022, **123**, 104198.
55 N. R. Mlyuka, G. A. Niklasson and C. G. Granqvist, *Sol. Energy Mater. Sol. Cells*, 2009, **93**, 1685–1687.
56 C. Liu, X. Cao, A. Kamyshny, J. Y. Law, S. Magdassi and Y. Long, *J. Colloid Interface Sci.*, 2014, **427**, 49–53.
57 S. Long, X. Cao, Y. Wang, T. Chang, N. Li, L. Jin, L. Ma, F. Xu, G. Sun and P. Jin, *Sol. Energy Mater. Sol. Cells*, 2020, **209**, 110449.
58 J. Rezek, J. Szelwicka, J. Vlček, R. Čerstvý, J. Houška, M. Fahland and J. Fahlteich, *Surf. Coat. Technol.*, 2022, **442**, 128273.
59 H. Guo, Y. G. Wang, H. R. Fu, A. Jain and F. G. Chen, *Ceram. Int.*, 2021, **47**, 21873–21881.
60 Y. Cui, S. Shi, L. Chen, H. Luo and Y. Gao, *Phys. Chem. Chem. Phys.*, 2015, **17**, 20998–21004.
61 H. Guo, Y. G. Wang, A. Jain, H. R. Fu and F. G. Chen, *J. Alloys Compd.*, 2021, **878**, 160352.
62 Z. Zhu, K. Zhu, J. Guo, Z. Fan, Z. Li and J. Zhang, *Colloid Interface Sci. Commun.*, 2022, **48**, 100619.
63 Q. Xu, Y. Ke, C. Feng, C. Chen, Z. Wen, H. Wang, M. Sun, X. Liu, H. Liu, S. Magdassi, H. Li, C. Huang and Y. Long, *Sol. Energy Mater. Sol. Cells*, 2021, **230**, 111163.
64 X. Wang, L. Chen, H. Lu, W. Fang, H. Li, W. Yin, M. Li, Y. Lu, P. Li and Y. He, *Appl. Phys. Lett.*, 2021, **118**, 192102.
65 M.-H. Lee and J.-S. Cho, *Thin Solid Films*, 2000, **365**, 5–6.
66 Z. Chen, Y. Gao, L. Kang, J. Du, Z. Zhang, H. Luo, H. Miao and G. Tan, *Sol. Energy Mater. Sol. Cells*, 2011, **95**, 2677–2684.
67 P. Jin, G. Xu, M. Tazawa and K. Yoshimura, *Jpn. J. Appl. Phys.*, 2002, **41**, 278.
68 C. Liu, S. Wang, Y. Zhou, H. Yang, Q. Lu, D. Mandler, S. Magdassi, C. Y. Tay and Y. Long, *J. Alloys Compd.*, 2018, **731**, 1197–1207.
69 L. Yao, Z. Qu, R. Sun, Z. Pang, Y. Wang, B. Jin and J. He, *ACS Appl. Energy Mater.*, 2019, **2**, 7467–7473.
70 S. Long, H. Zhou, S. Bao, Y. Xin, X. Cao and P. Jin, *RSC Adv.*, 2016, **6**, 106435–106442.
71 J. Zhu, A. Huang, H. Ma, Y. Chen, S. Zhang, S. Ji, S. Bao and P. Jin, *New J. Chem.*, 2017, **41**, 830–835.
72 J. Song, Y. Zhao, L. Sun, Q. Luo, H. Xu, C. Wang, H. Xin, W. Wu and F. Ma, *Ceram. Int.*, 2022, **48**, 15868–15876.
73 X. Zhou, Y. Ping, J. Gao, D. Gu, H. Zhou, M. Yang and Y. Jiang, *Appl. Surf. Sci.*, 2022, **597**, 153729.
74 J. Kang, J. Liu, F. Shi, Y. Dong, X. Song, Z. Wang, Z. Tian, J. Xu, J. Ma and X. Zhao, *Appl. Surf. Sci.*, 2022, **573**, 151507.
75 D. Li, S. Deng, Z. Zhao, J. Yang, B. Wang, J. Li and H. Jin, *Appl. Surf. Sci.*, 2022, **598**, 153741.
76 N. Shen, S. Chen, W. Wang, R. Shi, P. Chen, D. Kong, Y. Liang, A. Amini, J. Wang and C. Cheng, *J. Mater. Chem. A*, 2019, **7**, 4516–4524.
77 J. B. Kim, D. Lee, I. H. Yeo, H. Y. Woo, D. W. Kim, J.-Y. Chae, D. W. Lee, S. H. Han and T. Paik, *Sol. Energy Mater. Sol. Cells*, 2021, **226**, 111055.
78 A. Dong, J. Chen, P. M. Vora, J. M. Kikkawa and C. B. Murray, *Nature*, 2010, **466**, 474–477.
79 S. Long, X. Cao, R. Huang, F. Xu, N. Li, A. Huang, G. Sun, S. Bao, H. Luo and P. Jin, *ACS Appl. Mater. Interfaces*, 2019, **11**, 22692–22702.
80 K.-S. Kim, E.-W. Son, J. W. Youn and D. U. Kim, *Mater. Des.*, 2019, **176**, 107838.
81 G. Liu, S. Wang, A. I. Y. Tok, T. J. White, C. Li, M. Layani, S. Magdassi, M. Li and Y. Long, *ACS Omega*, 2019, **4**, 19635–19640.
82 J. Zhang, H. He, Y. Xie and B. Pan, *Phys. Chem. Chem. Phys.*, 2013, **15**, 4687–4690.
83 L. Chen, X. Wang, D. Wan, Y. Cui, B. Liu, S. Shi, H. Luo and Y. Gao, *RSC Adv.*, 2016, **6**, 73070–73082.
84 M. Jiang, Y. Li, S. Li, H. Zhou, X. Cao, S. Bao, Y. Gao, H. Luo and P. Jin, *J. Nanomater.*, 2014, **2014**, 183954.
85 G. Xu, P. Jin, M. Tazawa and K. Yoshimura, *Sol. Energy Mater. Sol. Cells*, 2004, **83**, 29–37.
86 S.-J. Kim, D. Lee, J.-Y. Chae, B. Ko, H. Lee, T. Paik and S.-H. Hong, *Appl. Surf. Sci.*, 2021, **565**, 150610.
87 Q. He, Y. Wang, Y. Zhou, M. He, R. Xu, S. Hu, W. Wu and R. Wang, *Opt. Mater.*, 2019, **97**, 109367.
88 T. D. Vu, X. Cao, H. Hu, J. Bao, T. Cao, J. Hu, X. Zeng and Y. Long, *Cell Rep. Phys. Sci.*, 2021, **2**, 100479.
89 Y. Ke, X. Wen, D. Zhao, R. Che, Q. Xiong and Y. Long, *ACS Nano*, 2017, **11**, 7542–7551.
90 H. Yuk, B. Lu and X. Zhao, *Chem. Soc. Rev.*, 2019, **48**, 1642–1667.
91 X. Liu, J. Liu, S. Lin and X. Zhao, *Mater. Today*, 2020, **36**, 102–124.
92 T. Zhou, H. Yuk, F. Hu, J. Wu, F. Tian, H. Roh, Z. Shen, G. Gu, J. Xu, B. Lu and X. Zhao, *Nat. Mater.*, 2023, **22**, 895–902.
93 Z. Sun, X. Xie, W. Xu, K. Chen, Y. Liu, X. Chu, Y. Niu, S. Zhang and C. Ren, *ACS Sustainable Chem. Eng.*, 2021, **9**, 12949–12959.
94 Q. Zhang, Y. Jiang, L. Chen, W. Chen, J. Li, Y. Cai, C. Ma, W. Xu, Y. Lu, X. Jia and Z. Bao, *Adv. Funct. Mater.*, 2021, **31**, 2100686.

 This journal is © The Royal Society of Chemistry 2024

Published on 25 April 2024. Downloaded by Yunnan University on 8/6/2025 12:09:49 AM.

95 Y. Feng, S. Wang, Y. Li, W. Ma, G. Zhang, M. Yang, H. Li, Y. Yang and Y. Long, *Adv. Funct. Mater.*, 2023, **33**, 2211027.
96 Y. Liu, J. Fan, R. Plamthottam, M. Gao, Z. Peng, Y. Meng, M. He, H. Wu, Y. Wang, T. Liu, C. Zhang and Q. Pei, *Chem. Mater.*, 2021, **33**, 7232–7241.
97 K. Wang, G. Chen, S. Weng, L. Hou, D. Ye and X. Jiang, *ACS Appl. Mater. Interfaces*, 2023, **15**, 4385–4397.
98 H. Zhang, J. Liu, F. Shi, T. Li, H. Zhang, D. Yang, Y. Li, Z. Tian and N. Zhou, *Chem. Eng. J.*, 2022, **431**, 133353.
99 L. Chen, G. Duan, C. Zhang, P. Cheng and Z. Wang, *Int. J. Extreme Manuf.*, 2022, **4**, 025302.
100 Y. Zhou, Y. Cai, X. Hu and Y. Long, *J. Mater. Chem. A*, 2014, **2**, 13550–13555.
101 K. Connelly, Y. Wu, X. Ma and Y. Lei, *Energies*, 2017, **10**, 1889.
102 Y.-S. Yang, Y. Zhou, F. B. Yin Chiang and Y. Long, *RSC Adv.*, 2016, **6**, 61449–61453.
103 X. Liu and Y. Wu, *Appl. Energy*, 2021, **303**, 117521.
104 M. Martin-Pastor and E. Stoyanov, *J. Polym. Sci.*, 2020, **58**, 1632–1641.
105 G. Vanti, M. Wang, M. C. Bergonzi, L. Zhidong and A. R. Bilia, *Int. J. Biol. Macromol.*, 2020, **164**, 232–241.
106 L. Zhang, H. Xia, F. Xia, Y. Du, Y. Wu and Y. Gao, *ACS Appl. Energy Mater.*, 2021, **4**, 9783–9791.
107 L. Zhang, Y. Du, H. Xia, F. xia, G. Yang and Y. Gao, *Ceram. Int.*, 2022, **48**, 37122–37131.
108 L. Zhang, Y. Du, F. Xia and Y. Gao, *Chem. Eng. J.*, 2023, **455**, 140849.
109 T.-G. La, X. Li, A. Kumar, Y. Fu, S. Yang and H.-J. Chung, *ACS Appl. Mater. Interfaces*, 2017, **9**, 33100–33106.
110 A. B. Ihsan, T. L. Sun, T. Kurokawa, S. N. Karobi, T. Nakajima, T. Nonoyama, C. K. Roy, F. Luo and J. P. Gong, *Macromolecules*, 2016, **49**, 4245–4252.
111 Y.-Q. Feng, M.-L. Lv, M. Yang, W.-X. Ma, G. Zhang, Y.-Z. Yu, Y.-Q. Wu, H.-B. Li, D.-Z. Liu and Y.-S. Yang, *Molecules*, 2022, **27**, 1638.
112 J. Li, P. Gu, H. Pan, Z. Qiao, J. Wang, Y. Cao, W. Wang and Y. Yang, *Adv. Sci.*, 2023, **10**, 2206044.
113 X. Wang and S. Narayan, *Front. Energy Res.*, 2021, **9**, 800382.
114 Y. Li, Y. Wang, J. Lu, W. Wang and D. Wang, *Chem. Eng. J.*, 2023, **457**, 141299.
115 B. Li, F. Xu, T. Guan, Y. Li and J. Sun, *Adv. Mater.*, 2023, **35**, 2211456.
116 S. Chen, G. Jiang, J. Zhou, G. Wang, Y. Zhu, W. Cheng, G. Xu, D. Zhao and H. Yu, *Adv. Funct. Mater.*, 2023, **33**, 2214382.
117 S. Dai, X. Dong, Y. Jiang, J. Ge, J. Ding and N. Yuan, *ACS Appl. Polym. Mater.*, 2023, **5**, 3398–3404.
118 G. Li, J. Chen, Z. Yan, S. Wang, Y. Ke, W. Luo, H. Ma, J. Guan and Y. Long, *Mater. Horiz.*, 2023, **10**, 2004–2012.
119 A. Roy, T. K. Mallick and A. A. Tahir, *J. Mater. Chem. C*, 2022, **10**, 15474–15482.
120 Z. Yu, Y. Yang, C. Shen, L. Mao, C. Cui, Z. Chen and Y. Zhang, *J. Mater. Chem. C*, 2023, **11**, 583–592.
121 G. Xu, H. Xia, P. Chen, W. She, H. Zhang, J. Ma, Q. Ruan, W. Zhang and Z. Sun, *Adv. Funct. Mater.*, 2022, **32**, 2109597.
122 J. Tian, H. Peng, X. Du, H. Wang, X. Cheng and Z. Du, *Prog. Org. Coat.*, 2021, **157**, 106287.
123 Y. Ding, Y. Duan, F. Yang, Y. Xiong and S. Guo, *Chem. Eng. J.*, 2023, **460**, 141572.
124 Y. Feng, W. Ma, H. Li, M. Yang, Y. Yu, S. Liu, X. Zeng, F. Huang, Y. Yang and Z. Li, *ACS Appl. Mater. Interfaces*, 2023, **15**, 5836–5844.
125 K. Wang, L. Zhang and X. Jiang, *J. Colloid Interf. Sci.*, 2023, **652**, 663–672.
126 Q. Lei, W. Yu, G. Xie, Y. Li, C. Wu, G. Jiang, Y. Zhou and H. Xie, *Sol. RRL*, 2023, **7**, 2200990.
127 J. Liu, R. Yang, J. Zhang, Q. Tao, A. Li, Z. Liu, Y. Su and Y. Liu, *Sol. Energy Mater. Sol. Cells*, 2023, **249**, 112048.
128 J. Tian, H. Peng, X. Du, H. Wang, X. Cheng and Z. Du, *J. Alloy. Compd.*, 2021, **858**, 157725.
129 Y. Zhou, M. Layani, S. Wang, P. Hu, Y. Ke, S. Magdassi and Y. Long, *Adv. Funct. Mater.*, 2018, **28**, 1705365.
130 Y. Wang, F. Zhao, J. Wang, L. Li, K. Zhang, Y. Shi, Y. Gao and X. Guo, *Nanomaterials*, 2019, **9**, 970.
131 R. Zhang, B. Xiang, Y. Shen, L. Xia, L. Xu, Q. Guan and S. Tang, *J. Mater. Chem. A*, 2021, **9**, 17481–17491.
132 M. Wu, Y. Shi, R. Li and P. Wang, *ACS Appl. Mater. Interfaces*, 2018, **10**, 39819–39827.
133 H. Y. Lee, Y. Cai, S. Bi, Y. N. Liang, Y. Song and X. M. Hu, *ACS Appl. Mater. Interfaces*, 2017, **9**, 6054–6063.
134 Y. Yao, Z. Xu, B. Liu, M. Xiao, J. Yang and W. Liu, *Adv. Funct. Mater.*, 2021, **31**, 2006944.
135 X. Zhu, W. Zhang, G. Lu, H. Zhao and L. Wang, *ACS Nano*, 2022, **16**, 16724–16735.
136 X. Wang, Y.-l. Wang, X. Yang, Z. Lu, Y. Men and J. Sun, *Macromolecules*, 2021, **54**, 10767–10775.
137 H. Li, F. Xu, T. Guan, Y. Li and J. Sun, *Nano Energy*, 2021, **90**, 106645.
138 L. Zheng, J. Zhang, H. Hua, Z. Wu, L. Wang and Y. Li, *Compos. Commun.*, 2023, **42**, 101684.
139 C. Nakamura, T. Yamamoto, K. Manabe, T. Nakamura, Y. Einaga and S. Shiratori, *Ind. Eng. Chem. Res.*, 2019, **58**, 6424–6428.
140 M. Dai, J. Zhao, Y. Zhang, H. Li, L. Zhang, Y. Liu, Z. Ye and S. Zhu, *ACS Appl. Mater. Interfaces*, 2022, **14**, 53314–53322.
141 M. Aburas, V. Soebarto, T. Williamson, R. Liang, H. Ebendorff-Heidepriem and Y. Wu, *Appl. Energy*, 2019, **255**, 113522.
142 K. E. Johnson, *Electrochem. Soc. Interface*, 2007, **16**, 38.
143 Y. Ma, M. Pharr, L. Wang, J. Kim, Y. Liu, Y. Xue, R. Ning, X. Wang, H. U. Chung, X. Feng, J. A. Rogers and Y. Huang, *Small*, 2017, **13**, 1602954.
144 H. Wang, G. Gurau and R. D. Rogers, *Chem. Soc. Rev.*, 2012, **41**, 1519–1537.
145 X. Sun, H. Luo and S. Dai, *Chem. Rev.*, 2012, **112**, 2100–2128.
146 M. Armand, F. Endres, D. R. MacFarlane, H. Ohno and B. Scrosati, *Nat. Mater.*, 2009, **8**, 621–629.
147 J. Zhu, A. Huang, H. Ma, Y. Ma, K. Tong, S. Ji, S. Bao, X. Cao and P. Jin, *ACS Appl. Mater. Interfaces*, 2016, **8**, 29742–29748.
148 H. Wu, M. Wang, W. Wu, D. Bai, Y. Liang, S. Hu, W. Yu, P. He and J. Zhang, *J. Mater. Chem. A*, 2023, **11**, 9626–9634.

Published on 25 April 2024. Downloaded by Yunnan University on 8/6/2025 12:09:49 AM.

149 Y. Qian, C. Chai, P. Qi, L. Ma and J. Hao, *ACS Appl. Polym. Mater.*, 2023, **5**, 2983–2994.
150 B. Deng, Y. Zhu, X. Wang, J. Zhu, M. Liu, M. Liu, Y. He, C. Zhu, C. Zhang and H. Meng, *Adv. Mater.*, 2023, **35**, 2302685.
151 X. Zhang, L. B. Abdalla, Q. Liu and A. Zunger, *Adv. Funct. Mater.*, 2017, **27**, 1701266.
152 W. Tian, H. Zhou and L. Li, *Small*, 2017, **13**, 1702107.
153 J. S. Manser, M. I. Saidaminov, J. A. Christians, O. M. Bakr and P. V. Kamat, *Acc. Chem. Res.*, 2016, **49**, 330–338.
154 S. Liu, Y. Li, Y. Wang, K. M. Yu, B. Huang and C. Y. Tso, *Adv. Sci.*, 2022, **9**, 2106090.
155 C. Li, R. Tao, Y. Ding, C. Liu, X. Ding, H. Xu, C. Zhi, C. Jia and Z. Li, *Sol. RRL*, 2022, **6**, 2101009.
156 B. A. Rosales, J. Kim, V. M. Wheeler, L. E. Crowe, K. J. Prince, M. Mirzokarimov, T. Daligault, A. Duell, C. A. Wolden, L. T. Schelhas and L. M. Wheeler, *Adv. Energy Mater.*, 2023, **13**, 2203331.
157 S.-H. Wu, G. Cossio, B. Braun, F. C. M. Wu and E. T. Yu, *Adv. Opt. Mater.*, 2023, **11**, 2202409.
158 Y. Liu, J. Wang, F. Wang, Z. Cheng, Y. Fang, Q. Chang, J. Zhu, L. Wang, J. Wang, W. Huang and T. Qin, *Nat. Commun.*, 2021, **12**, 3360.
159 N. Ahn, S. M. Kang, J.-W. Lee, M. Choi and N.-G. Park, *J. Mater. Chem. A*, 2015, **3**, 19901–19906.
160 G. Teri, Q.-Q. Jia, Q.-F. Luo, H.-F. Ni, D.-W. Fu and Q. Guo, *J. Mater. Chem. C*, 2023, **11**, 8903–8907.
161 S. Liu, Y. W. Du, C. Y. Tso, H. H. Lee, R. Cheng, S.-P. Feng and K. M. Yu, *Adv. Funct. Mater.*, 2021, **31**, 2010426.
162 K. Binnemans, *Chem. Rev.*, 2005, **105**, 4148–4204.
163 S.-W. Oh, S.-M. Ji, C.-H. Han and T.-H. Yoon, *Dyes Pigm.*, 2022, **197**, 109843.
164 G. H. Timmermans, J. Wu, A. P. H. J. Schenning, J. Lin and M. G. Debije, *Adv. Photonics Res.*, 2021, **2**, 2100134.
165 L. Wang, A. M. Urbas and Q. Li, *Adv. Mater.*, 2020, **32**, 1801335.
166 Y. Ke, J. Chen, G. Lin, S. Wang, Y. Zhou, J. Yin, P. S. Lee and Y. Long, *Adv. Energy Mater.*, 2019, **9**, 1902066.
167 W. Shen and G. Li, *Laser Photonics Rev.*, 2023, **17**, 2200207.
168 X. Li, M. Zhang, C. Zhang, R. Niu, H. Ma and Y. Sun, *Opt. Mater.*, 2023, **138**, 113659.
169 A. Ghosh, *Energy*, 2023, **265**, 126396.
170 P. Yu, Z. He, Y. Zhao, H. Zhang, H. Zhang, Z. Miao and W. Shen, *Appl. Mater. Today*, 2023, **30**, 101724.
171 X. Liang, M. Chen, Q. Wang, S. Guo, L. Zhang and H. Yang, *J. Mater. Chem. C*, 2018, **6**, 7054–7062.
172 X. Liang, C. Guo, M. Chen, S. Guo, L. Zhang, F. Li, S. Guo and H. Yang, *Nanoscale Horiz.*, 2017, **2**, 319–325.
173 J. Sun and S.-T. Wu, *J. Polym. Sci., Part B: Polym. Phys.*, 2014, **52**, 183–192.
174 S.-M. Guo, X. Liang, C.-H. Zhang, M. Chen, C. Shen, L.-Y. Zhang, X. Yuan, B.-F. He and H. Yang, *ACS Appl. Mater. Interfaces*, 2017, **9**, 2942–2947.
175 I. Dierking, *Adv. Mater.*, 2000, **12**, 167–181.
176 W. Meng, Y. Gao, X. Hu, L. Tan, L. Li, G. Zhou, H. Yang, J. Wang and L. Jiang, *ACS Appl. Mater. Interfaces*, 2022, **14**, 28301–28309.
177 X. Liang, M. Chen, S. Guo, L. Zhang, F. Li and H. Yang, *ACS Appl. Mater. Interfaces*, 2017, **9**, 40810–40819.
178 H. Y. Lee, Y. Cai, S. Velioglu, C. Mu, C. J. Chang, Y. L. Chen, Y. Song, J. W. Chew and X. M. Hu, *Chem. Mater.*, 2017, **29**, 6947–6955.
179 Y. Zhang, K. Wu and Q. Fu, *Adv. Funct. Mater.*, 2022, **32**, 2109255.
180 W. Li, X. Li, J. Liu, M.-j. Zeng, X. Feng, X. Jia and Z.-Z. Yu, *ACS Appl. Mater. Interfaces*, 2021, **13**, 22845–22854.
181 W. Li, X. Tian, X. Li, S. Han, C. Li, X.-Z. Zhai, Y. Kang and Z.-Z. Yu, *J. Mater. Chem. A*, 2021, **9**, 14859–14867.
182 W. Li, X. Tian, X. Li, J. Liu, C. Li, X. Feng, C. Shu and Z.-Z. Yu, *J. Colloid Interface Sci.*, 2022, **606**, 748–757.
183 P. K. Nayak, S. Mahesh, H. J. Snaith and D. Cahen, *Nat. Rev. Mater.*, 2019, **4**, 269–285.
184 Z. Xie, X. Jin, G. Chen, J. Xu, D. Chen and G. Shen, *Chem. Commun.*, 2014, **50**, 608–610.
185 L. L. Baranowski, G. J. Snyder and E. S. Toberer, *Energy Environ. Sci.*, 2012, **5**, 9055–9067.
186 D. Kraemer, B. Poudel, H.-P. Feng, J. C. Caylor, B. Yu, X. Yan, Y. Ma, X. Wang, D. Wang, A. Muto, K. McEnaney, M. Chiesa, Z. Ren and G. Chen, *Nat. Mater.*, 2011, **10**, 532–538.
187 C. Shu, H.-Y. Zhao, S. Zhao, W. Deng, P. Min, X.-H. Lu, X. Li and Z.-Z. Yu, *Composites, Part B*, 2023, **248**, 110367.
188 F. Guo, S. Chen, Z. Chen, H. Luo, Y. Gao, T. Przybilla, E. Spiecker, A. Osvet, K. Forberich and C. J. Brabec, *Adv. Opt. Mater.*, 2015, **3**, 1524–1529.
189 K. Wang, H. Wu, Y. Meng, Y. Zhang and Z. Wei, *Energy Environ. Sci.*, 2012, **5**, 8384–8389.
190 Y. Meng, X. Li, S. Wang, C. Lau, H. Hu, Y. Ke, G. Tan, J. Yang and Y. Long, *Nano Energy*, 2022, **91**, 106632.
191 Y. Niu, Y. Zhou, D. Du, X. Ouyang, Z. Yang, W. Lan, F. Fan, S. Zhao, Y. Liu, S. Chen, J. Li and Q. Xu, *Adv. Sci.*, 2022, **9**, 2105184.
192 Y. Meng, Y. Tan, X. Li, Y. Cai, J. Peng and Y. Long, *Appl. Energy*, 2022, **324**, 119676.

 This journal is © The Royal Society of Chemistry 2024